Evaluation of the MACC operational forecast system- potential and challenges of global near-real-time modelling with respect to reactive gases in the troposphere

A. Wagner1, A.–M. Blechschmidt2, I. Bouarar3[*], E.-G. Brunke4, C. Clerbaux3, M. Cupeiro5, P. Cristofanelli6, H. Eskes7, J. Flemming8, H. Flentje1, M. George3, S. Gilge1, A. Hilboll2, A. Inness8, J. Kapsomenakis9, A. Richter2, L. Ries10, W. Spangl11, O. Stein12, R. Weller13, C. Zerefos9

[1]{Deutscher Wetterdienst, Meteorologisches Observatorium Hohenpeissenberg, Germany}

[2]{Institute of Environmental Physics, University of Bremen, Germany}

[3]{Sorbonne Universités, UPMC Univ. Paris 06; Université Versailles St-Quentin; CNRS/INSU, LATMOS-IPSL, Paris, France}

[4]{South African Weather Service, Stellenbosch, South Africa}

[5]{National Meteorological Service, Ushuaia, Tierra del Fuego, Argentina}

[6]{National Research Council of Italy, ISAC, Bologna, Italy}

[7]{Royal Netherlands Meteorological Institute, De Bilt, The Netherlands}

[8]{European Centre for Medium-range Weather Forecasts, Reading, UK}

[9]{Academy of Athens, Research Centre for Atmospheric Physics and Climatology, Athens, Greece}

[10]{Federal Environment Agency, GAW Global Station Zugspitze/Hohenpeissenberg, Zugspitze 5, D-82475 Zugspitze}

[11]{Umweltbundesamt GmbH, Air Pollution Control & Climate Change Mitigation, Vienna, Austria}

[12]{Forschungszentrum Jülich, IEK-8 (Troposphere), Jülich, Germany}

[13]{Alfred Wegener Institute, Bremerhaven, Germany}

1   [*]{now at: Max-Planck-Institut for Meteorology, Hamburg, Germany}

2   Correspondence to: A. Wagner (Annette.wagner@dwd.de)

3

4   **Abstract**

5   Monitoring Atmospheric Composition and Climate (MACC) currently represents the

6   European Union's Copernicus Atmosphere Monitoring Service (CAMS)

7   (http://www.copernicus.eu/), which will become fully operational in the course of 2015. The

8   global near-real-time MACC model production run for aerosol and reactive gases provides

9   daily analyses and 5-day forecasts of atmospheric composition fields. It is the only

10   assimilation system world-wide that is operational to produce global analyses and forecasts of

11   reactive gases and aerosol fields. We have investigated the ability of the MACC analysis

12   system to simulate tropospheric concentrations of reactive gases (CO, O_3, and NO_2) covering

13   the period between 2009 and 2012. A validation was performed based on CO and O_3 surface

14   observations from the Global Atmosphere Watch (GAW) network, O_3 surface observations

15   from the European Monitoring and Evaluation Programme (EMEP) and furthermore, NO_2

16   tropospheric columns derived from the satellite sensors SCIAMACHY and GOME-2, and CO

17   total columns derived from the satellite sensor MOPITT. The MACC system proved capable

18   of reproducing reactive gas concentrations in consistent quality, however, with a seasonally

19   dependent bias compared to surface and satellite observations: For northern hemisphere

20   surface O_3 mixing ratios, positive biases appear during the warm seasons and negative biases

21   during the cold parts of the years, with monthly Modified Normalised Mean Biases (MNMBs)

22   ranging between -30% and 30% at the surface. Model biases are likely to result from

23   difficulties in the simulation of vertical mixing at night and deficiencies in the model's dry

24   deposition parameterization. Observed tropospheric columns of NO_2 and CO could be

25   reproduced correctly during the warm seasons, but are mostly underestimated by the model

26   during the cold seasons, when anthropogenic emissions are at a highest, especially over the

27   US, Europe and Asia. Monthly MNMBs of the satellite data evaluation range between -110%

28   and 40% for NO_2 and at most -20% for CO, over the investigated regions. The

29   underestimation is likely to result from a combination of errors concerning the dry deposition

30   parameterization and certain limitations in the current emission inventories, together with an

31   insufficiently established seasonality in the emissions.

1 Introduction

The impact of reactive gases on climate, human health and environment has gained increasing public and scientific interest in the last decade (Bell et al., 2006, Cape 2008, Mohnen et al., 2013, Seinfeld and Pandis 2006, Selin et al., 2009). As air pollutants, carbon monoxide (CO), nitrogen oxides (NO_x) and ozone (O_3) are known to have acute and chronic effects on human health, ranging from minor upper respiratory irritation to chronic respiratory and heart disease, lung cancer, acute respiratory infections in children and chronic bronchitis in adults (Bell et al., 2006, Kampa and Castanas 2006). Tropospheric ozone, even in small concentrations, is also known to cause plant damage in reducing plant primary productivity and crop yields (e.g. Ashmore 2005). It is also contributing to global warming by direct and indirect radiative forcing (Forster et al., 2007, Sitch et al., 2007). Pollution events can be caused by local sources and processes but are also influenced by continental and intercontinental transport of air masses. Global models can provide the transport patterns of air masses and deliver the boundary conditions for regional models, facilitating the forecast and investigation of air pollutants.

The EU-funded research project MACC - Monitoring Atmospheric Composition and Climate, (consisting of a series of European projects, MACC to MACC-III), provides the preparatory work that will form the basis of the Copernicus Atmosphere Monitoring Service (CAMS). This service is established by the EU to provide a range of products of societal and environmental value with the aim to help European governments respond to climate change and air quality problems. MACC provides reanalysis, monitoring products of atmospheric key constituents (e.g. Inness et al., 2013), as well as operational daily forecasting of greenhouse gases, aerosols and reactive gases (Benedetti et al., 2011, Stein et al., 2012) on a global and on European-scale level, and derived products such as solar radiation. An important aim of the MACC system is to describe the occurrence, magnitude and transport pathways of disruptive events, e.g., volcanoes (Flemming and Inness, 2013), major fires (Huijnen et al., 2012, Kaiser et al., 2012) and dust storms (Cuevas et al., 2015). The product catalogue can be found on the MACC website, http://copernicus-atmosphere.eu. For the generation of atmospheric products, state-of-the-art atmospheric modelling is combined with assimilated satellite data (Hollingsworth et al., 2008, Inness et al., 2013, 2015, more general information about data assimilation can be found in e.g. Ballabrera-Poy et al., 2009 or Kalnay 2003). Within the MACC project there is a dedicated validation activity to provide up-to-date

information on the quality of the reanalysis, daily analyses and forecasts. Validation reports are updated regularly and are available on the MACC websites.

The MACC global near-real-time (NRT) production model for reactive gases and aerosol has operated with data assimilation from September 2009 onwards, providing boundary conditions for the MACC regional air quality products (RAQ), and other downstream users. The model simulations also provide input for the stratospheric ozone analyses delivered in near-real-time by the MACC stratospheric ozone system (Lefever et al., 2014).

In this paper we describe the investigation of the potential and challenges of near-real-time modelling with the MACC analysis system between 2009 and 2012. We concentrate on this period because of the availability of validated independent observations (namely surface observations from the Global Atmosphere Watch Programme GAW, the European Monitoring and Evaluation Programme EMEP, as well as total column satellite data from the MOPITT, SCIAMACHY and GOME-2 sensors) that are used for comparison. In particular, we study the model's ability to reproduce the seasonality and absolute values of CO and NO_2 in the troposphere as well as O_3 and CO at the surface. The impact of changes in model version, data assimilation and emission inventories on the model performance is examined and discussed. The paper is structured in the following way: Section 2 contains a description of the model and the validation data sets as well as the applied validation metrics. Section 3 presents the validation results for CO, NO_2 and O_3. Section 4 provides the discussion and section 5 the conclusions of the paper.

2   Data and Methods

2.1 The MACC model system in the 2009-2012 period

The MACC global products for reactive gases consist of a reanalysis performed for the years 2003-2012 (Inness et al., 2013) and the near-real-time analysis and forecast, largely based on the same assimilation and forecasting system, but targeting different user groups. The MOZART chemical transport model (CTM) is coupled to the Integrated Forecast System (IFS) of the European Centre for Medium-Range Weather forecast (ECMWF), which together represent the MOZART-IFS model system (Flemming et al., 2009 and Stein et al. 2012). An alternative analysis system has been set up based on the global CTM TM5 (Huijnen et al., 2010). Details of the MOZART version used in the MACC global products can be found in Kinnison et al., 2007 and Stein et al. (2011, 2012). In the simulation, the IFS and the

4

MOZART model run in parallel and exchange several two- and three-dimensional fields every model hour using the OASIS4 coupling software (Valcke and Redler 2006), thereby producing three-dimensional IFS fields for O_3, CO, SO_2, NO_x, HCHO, sea salt aerosol, desert dust, black carbon, organic matter, and total aerosol. The IFS provides meteorological data to MOZART. Data assimilation and transport of the MACC species takes place in IFS, while the whole chemical reaction system is calculated in MOZART.

The MACC_osuite (operational suite) is the global near-real-time MACC model production run for aerosol and reactive gases. Here, we have investigated only the MACC analysis. In contrast to the reanalysis, the MACC_osuite is a near-real-time run, which implies that it is only run once in near-real-time and may thus contain inconsistencies in e.g. the assimilated data. The MACC_osuite was based on the IFS cycle CY36R1 with IFS model resolution of approximately 100 km by 100 km at 60 levels (T159L60) from September 2009 until July 2012. The gas-phase chemistry module in this cycle is based on MOZART-3 (Kinnison et al., 2007). The model has been upgraded, following updates of the ECMWF meteorological model and MACC-specific updates, i.e. in chemical data assimilation and with respect to the chemical model itself. Thus, from July 2012 onwards, the MACC_osuite has run with a change of the meteorological model to a new IFS cycle (version CY37R3), with an IFS model resolution of approximately 80 km at 60 levels (T255L60) and an upgrade of the MOZART version 3.5 (Kinnison et al., 2007; Emmons et al., 2011, Stein et al. 2013). This includes, amongst others, updated velocity fields for the dry deposition of O_3 over ice, as described in Stein et al. (2013). A detailed documentation of system changes can be found at:

http://www.copernicus-atmosphere.eu/oper_info/nrt_info_for_users/

2.1.1 Emission inventories and assimilated data sets

In the MACC_osuite, anthropogenic emissions are based on emissions out of the EU project RETRO merged with updated emissions for East Asia from the REAS inventory, (Schultz et al. 2007) in the following referred to as RETRO-REAS. The horizontal resolution is 0.5° in latitude and longitude and it contains a monthly temporal resolution. Biogenic emissions are taken from GEIA, fire emissions are based on a climatology derived from GFEDv2 (van der Werf et al., 2006) until April 2010, when fire emissions change to GFAS fire emissions (Kaiser et al., 2012). Between January 2011 and October 2011 there has been a fire emission

1　reading error in the model, where, instead of adjusting emissions to the appropriate month, the

2　same set of emissions have been read throughout this period.

3　After the model upgrade to the new cycle version CY37R3, in July 2012, the emission

4　inventories changed from the merged RETRO-REAS and GEIA inventories, used in the

5　previous cycle, to the MACCity anthropogenic and biogenic emissions (Granier et al., 2011)

6　and (climatological) MEGAN-v2 (Guenther et al., 2006) emission inventories. Wintertime

7　anthropogenic CO emissions are scaled up over Europe and North America (see Stein et al.,

8　2014). Near-real-time fire emissions are taken from GFASv1.0 (Kaiser et al. 2012), for both

9　gas-phase and aerosol.

10　In the MACC_osuite, the initial conditions for some of the chemical species are provided by

11　data assimilation of atmospheric composition observations from satellites (see Benedetti et

12　al., 2009; Inness et al., 2009, 2013; Massart et al., 2014). Table 1 lists the assimilated data

13　products. From September 2009 to June 2012, O_3 total columns of the MLS and SBUV-2

14　instruments are assimilated, as well as OMI and SCIAMACHY total columns (the latter only

15　until March 2012, when the European Space Agency lost contact with the ENVIronmental

16　SATellite ENVISAT). CO total columns are assimilated from the IASI sensor and aerosol

17　total optical depth is assimilated from the MODIS instrument. After the model cycle update in

18　July 2012, data assimilation also contains OMI tropospheric columns of NO_2 and SO_2, as well

19　as CO MOPITT total columns. The CO total columns retrieved by MOPITT and IASI

20　instruments have a relatively similar seasonality, but there is a systematic difference with

21　MOPITT CO being higher over most regions in the northern hemisphere, especially during

22　winter and spring. George et al. ("An examination of the long-term CO records from

23　MOPITT and IASI and comparison of retrieval methodology", AMTD, 2015 submitted)

24　investigated the differences between MOPITT and IASI, and showed the impact of a priori

25　information on the retrieved measurements.

26　Table 1 and 2 summarize the data assimilation and setup of the MACC_osuite.

2.2 Validation data and methodology

28　In this study, mainly the same evaluation data sets have been used as during the MACC near-

29　real-time validation exercise. This implies some discontinuities in the evaluations, e.g. the

30　substitution of SCIAMACHY data with GOME-2 data after the loss of the ENVISAT sensor

31　or an exclusion of MOPITT satellite data after the start of its assimilation into the model. The

continuous process of updating and complementation of data sets in databases requires the selection and definition of an evaluation data set at some point. The comparatively small inconsistencies between our data sets are considered to have a negligible impact on the overall evaluation results.

2.2.1 GAW Surface O$_3$ and CO Observations

The Global Atmosphere Watch (GAW) programme of the World Meteorological Organization (WMO) has been established to provide reliable long-term observations of the chemical composition and physical properties of the atmosphere, which are relevant for understanding atmospheric chemistry and climate change (WMO, 2013). GAW tropospheric O$_3$ measurements are performed in a way to be suitable for the detection of long-term regional and global changes. Furthermore, the GAW measurement programme focuses on observations, which are regionally representative and should be free from influence of significant local pollution sources and suited for the validation of global chemistry climate models (WMO 2007). Detailed information on GAW and GAW related O$_3$ and CO measurements can be found in WMO (2010, 2013).

Hourly O$_3$ and CO data have been downloaded from the WMO/GAW World Data Centre for Greenhouse Gases (WDCGG) for the period between 09/2009 and 12/2012 (status of download: 07/2013). Our evaluation includes 29 stations with surface observations for CO and 50 stations with surface observations for O$_3$. Table 3 lists the geographic coordinates and altitudes of the individual stations. Being a long-term data network, the data in the database is provided with a temporal delay of approximately 2 years. As the data in the database becomes sparse towards the end of the validation period, near-real-time observations, as used in the MACC-project for near-real-time validation, presented on the MACC website, have been included to complement the validation data sets. For the detection of long-term trends and year-to-year variability, the data quality objectives (DQOs) for CO in GAW measurements are set to a maximum uncertainty of $\pm$ 2 ppb and to $\pm$ 5 ppb for marine boundary layer sites and continental sites that are influenced by regional pollution and to $\pm$ 1 ppb for ozone (WMO, 2012, 2013).

For the evaluation with GAW station data, 6-hourly values (0, 6, 12, 18 UTC) of the analysis mode have been extracted from the model and are matched with hourly observational GAW station data. Model mixing ratios at the stations' location have been linearly interpolated from the model data in the horizontal. In the vertical, modelled gas mixing ratios have been

7

extracted at the model level, which is closest to the GAW stations' altitude. Validation scores (see section 2.3) have been calculated for each station between the 6-hourly model analysis data and the corresponding observational data for the entire period (09/2009- 12/2012) and as monthly averages.

2.2.2 EMEP Surface O₃ Observations

The European Monitoring and Evaluation Programme (EMEP) is a scientifically based and policy driven programme under the Convention on Long-Range Transboundary Air Pollution (CLRTAP) for international co-operation to solve transboundary air pollution problems. Measurements of air quality in Europe have been carried out under the EMEP since 1977. A detailed description of the EMEP measurement programme can be found in Tørseth et al. (2012). The surface hourly ozone data between 09/2009 and 12/2012 have been downloaded from the EMEP data web-page (http://www.nilu.no/projects/ccc/emepdata.html). For the validation, only stations meeting the 75% availability threshold per day and per month are taken into account. The precision is close to 1.5 ppb for a 10s measurement. More information about the ozone data quality, calibration and maintenance procedures can be found in Aas et al. (2000).

For comparison with EMEP data, 3-hourly model values (0, 3, 6, 12, 15, 18, 21 UTC) of the analysis mode have been chosen, in order to be able to evaluate day and night time performance of the model separately. Gas mixing ratios have been extracted from the model and are matched with hourly observational surface ozone data at 124 EMEP stations in the same way as for the GAW station data. The EMEP surface ozone values and the interpolated surface modeled values are compared on a monthly basis for the latitude bands of $30^{o}N$ – $40^{o}N$ (southern Europe), $40^{o}N$ – $50^{o}N$ (central Europe) and $50^{o}N$ – $70^{o}N$ (northern Europe). For the identification of differences in the MACC_osuite performance between day and night time, the MACC_osuite simulations and the EMEP observations for the three latitude bands have been additionally separated into day-time (12:00–15:00 Local Time LT) and night-time (00:00–03:00 LT) intervals.

2.2.3 MOPITT CO total column retrievals

The MOPITT (Measurement Of Pollution In The Troposphere) instrument is mounted on board the NASA EOS Terra satellite and provides CO distributions at the global scale (Deeter et al., 2004). MOPITT has a horizontal resolution of 22 km x 22 km and allows global

coverage within 3 days. The data used in this study corresponds to CO total columns from version 5 (V5) of the MOPITT thermal infrared (TIR) product level 3. This product is available via the following web server: http://www2.acd.ucar.edu/mopitt/products. Validation of the MOPITT V5 product against in-situ CO observations showed a mean bias of 0.06×10^{18} molecules cm^{-2} (Deeter et al., 2013). Following the recommendation in the users' guide, (www.acd.ucar.edu/mopitt/v5_users_guide_beta.pdf), the MOPITT data were averaged by taking into account their relative errors provided by the Observation Quality Index (OQI).

Also, in order for better data quality we used only daytime CO data since retrieval sensitivity is greater for daytime rather than nighttime overpasses. A further description of the V5 data is presented in Deeter et al. (2013) and Worden et al. (2014).

For the validation, the model CO profiles (X) were transformed by applying the MOPITT averaging kernels (A) and the a priori CO profile (X_a) according to the following equation (Rodgers, 2000) to derive the smoothed profiles X* appropriate for comparison with MOPITT data:

$$X^*=X_a + A(X - X_a)$$

Details on the method of calculation are referred to in Deeter et al. (2004) and Rodgers (2000). The averaging kernels indicate the sensitivity of the MOPITT measurement and retrieval system to the true CO profile, with the remainder of the information set by the a priori profile and retrieval constraints (Emmons, 2009; Deeter et al., 2010). The model CO total columns used in the comparison with MOPITT observations, have been calculated using the averaging kernel smoothed profiles X* which have the same vertical resolution and a priori dependence as the MOPITT retrievals. For the evaluation, 8 regions are defined (see Fig. 1): Europe, Alaska, Siberia, North Africa, South Africa, South Asia, East Asia and the United States.

The model update in July 2012 includes an integration of MOPITT CO total columns in the model's data assimilation system. With this, the MOPITT validation data has lost its independency for the rest of the validation period and MOPITT validation data has thus only been used until June 2012 for validation purposes.

2.2.4 SCIAMACHY and GOME-2 NO$_2$ Satellite Observations

The SCanning Imaging Absorption spectroMeter for Atmospheric CHartographY (SCIAMACHY; Bovensmann et al., 1999) onboard the ENVISAT and the Global Ozone

1 Monitoring Experiment-2 (GOME-2; Callies et al., 2000) onboard the Meteorological

2 Operational Satellite-A (MetOp-A) comprise UV-VIS and NIR sensors designed to provide

3 global observations of atmospheric trace gases.

4 In this study, the tropospheric NO_2 column data set described in Hilboll et al. (2013a) has

5 been used. In short, the measured radiances are analysed using Differential Optical

6 Absorption Spectroscopy (DOAS), (Platt and Stutz, 2008) in the 425–450 nm wavelength

7 window (Richter and Burrows, 2002). The influence of stratospheric NO_2 air masses has been

8 accounted for using the algorithm detailed by Hilboll et al. (2013b), using stratospheric NO_2

9 fields from the B3dCTM model (Sinnhuber at al., 2003a; Sinnhuber et al., 2003b; Winkler et

10 al., 2008). Tropospheric air mass factors have been calculated with the radiative transfer

11 model SCIATRAN (Rozanov et al., 2005). Only measurements with FRESCO+ algorithm

12 (Wang et al., 2008) cloud fractions of less than 20% are used.

13 Tropospheric NO_2 vertical column densitiy (VCD) from the MACC_osuite is compared to

14 tropospheric NO_2 VCD from GOME-2 and SCIAMACHY. As the European Space Agency

15 lost contact with ENVISAT in April 2012, GOME-2 data is used for model validation from 1

16 April 2012 onwards, while SCIAMACHY data is used for the remaining time period

17 (September 2009 to March 2012). Satellite observations are gridded to the horizontal model

18 resolution, i.e. 1.875° for IFS cycle CY36R1 (09/2009 -06/2012) and 1.125° for cycle

19 CY37R3 (07/2012- 12/2012).

20 A few processing steps are applied to the MACC_osuite data to account for differences to the

21 satellite data such as observation time. Firstly, model data are vertically integrated to

22 tropospheric NO_2 VCDs by applying National Centers for Environmental Prediction (NCEP)

23 reanalysis (Kalnay et al., 1996) climatological tropopause pressure shown in Fig.1 of Santer et

24 al. (2003). Secondly, simulations are interpolated linearly in time to the SCIAMACHY

25 equator crossing time (roughly 10:00 LT). This most likely leads to some minor

26 overestimation of model NO_2 VCDs compared to GOME-2 data, as the equator crossing time

27 for GOME-2 is about 9:30 LT. Moreover, only model data for which corresponding satellite

28 observations exist are considered. For the evaluation, the same regions have been used as for

29 MOPITT (Fig.1), except for Siberia and Alaska. In contrast to MOPITT data, no averaging

30 kernel is applied.

31 Satellite observations of tropospheric NO_2 columns have relatively large uncertainties, mainly

32 linked to incomplete stratospheric correction (important over clean regions and at high

1 latitudes in winter and spring) and to uncertainties in air mass factors (mainly over polluted

2 regions) (e.g. Boersma et al., 2004 and Richter et al., 2005). The uncertainty varies with

3 geolocation and time but in first approximation can be separated into an absolute error of

4 5×10^{14} molec cm^{-2} and a relative error of about 30%, whichever is larger. As some of the

5 contributions to this uncertainty are systematic, averaging over longer time periods does not

6 reduce the errors as much as one would expect for random errors. Over polluted regions, the

7 uncertainty from random noise in the spectra is small in comparison to other error sources, in

8 particular for monthly averages.

9 **2.3 Validation metrics**

10 A comprehensive model evaluation requires the selection of validation metrics that provide

11 complementary aspects of model performance. The following metrics have been used in the

12 evaluation:

13 **Modified Normalized Mean Bias MNMB**

14
$$MNMB = \frac{2}{N} \sum_i \frac{f_i - o_i}{f_i + o_i} \qquad (1)$$

15 **Root Mean Square Error RMSE**

16
$$RMSE = \sqrt{\frac{1}{N} \sum_i (f_i - o_i)^2} \qquad (2)$$

17 **Correlation Coefficient**

18
$$R = \frac{\frac{1}{N} \sum_i (f_i - \bar{f})(o_i - \bar{o})}{\sigma_f \sigma_o} \qquad (3)$$

19 where: N is the number of observations, f are the modelled analysis and o the observed

20 values, $\bar{f}$ and $\bar{o}$ are the mean values of the analysis and observed values and σ_f and σ_o

21 are the corresponding standard deviations.

22 The validation metrics above have been chosen to provide complementary aspects of model

23 performance. The modified normalized mean bias is a normalization based on the mean of the

24 observed and forecast value (e.g. Elguindi et al. 2010). It ranges between

25 -2 and 2 and is very useful to check whether there is a negative or positive deviation between

model and observations. When multiplied by 100%, it can be interpreted as a percentage bias. The advantage of the MNMB is that it varies symmetrically with respect to under- and overestimation and is robust with respect to outliers. However, when calculated over longer time periods, a balance in model error, with model over-and underestimation compensating each other, can lead to a small MNMB for the overall period. For this reason, it is important to additionally consider an absolute measure, such as the RMSE. However, it has to be noted that the RMSE is strongly influenced by larger values and outliers, due to squaring. The correlation coefficient R can vary between 1 (perfect correlation) and -1 (negative correlation) and is an important measure to check the linearity between model and observations.

3   Results

3.1 Evaluation of Ozone

The evaluation of the MACC_osuite run with O_3 from GAW surface observations (described in section 2.2.1) demonstrates good agreement in absolute values and seasonality for most regions. Figure 2 shows maps with Modified Normalized Mean Bias (MNMB, see section 2.3) evaluations for 50 GAW stations globally (top) and in Europe (below). Figure 3 presents selected time series plots representing the results for high latitudes, low latitudes and Europe. Large negative MNMBs over the whole period 09/2009 to 12/2012 (-30 to -82%) are observed for stations located in Antarctica (Neumayer-NEU, South Pole-SPO, Syowa-SYO and Concordia- CON) whereby O_3 surface mixing ratios are strongly underestimated by the model. For stations located in high latitudes in the northern hemisphere (Barrow-BAR, Alaska and Summit-SUM, Denmark), the MACC_osuite exhibits similar underestimated values of up to -35% for the whole evaluation period. The time series plots for Arctic and Antarctic stations (e.g. Summit-SUM, Neumayer-NEU and South Pole-SPO) in Fig. 3 show that an underestimation visible in these regions has been remedied and model performance improved with an updated dry deposition parameterization over ice, which has been introduced with the new model cycle in July 2012 (see section 2.1).

Large positive MNMBs (up to 50 to 70%, Fig. 2) are observed for stations that are located in or nearby cities and thus exposed to regional sources of contamination (Iskrba-ISK Slovenia, Tsukuba- TSU, Japan, Cairo-CAI, Egypt). In tropical and subtropical regions, O_3 surface mixing ratios are systematically overestimated (by about 20% on average) during the evaluation period. The time series plots for tropical and subtropical stations (e.g. for Ragged

Point-RAG, Barbados and Cape Verde Observatory, Cape Verde –CVO, Fig. 3) reveal a slight systematic positive offset throughout the year, however with high correlation coefficients (0.6 on average).

For GAW stations in Europe, the evaluation of the MACC_osuite for the whole period shows MNMBs between -80 and 67%. Large biases appear only for 2 GAW stations located in Europe: Rigi- RIG, Switzerland (-80%), located near mountainous terrain and Iskrba- ISK, Slovenia (67%). For the rest of the stations MNMBs lie between 22 and -30%. Root Mean Square Errors (RMSEs, see section 2.3) range between 7 and 35 ppb (15 ppb on average). Again, results for Iskrba-ISK and Rigi-RIG show the largest errors. All other stations show RMSEs between 7 and 20 ppb. Correlation coefficients here range between 0.1 and 0.7 (with 0.5 on average). Table 4 summarizes the results for all stations individually.

Monthly MNMBs (see Fig. 4) show a seasonally varying bias, with positive MNMBs occurring during the northern summer months (with global average ranging between 5 and 29% during the months June and October), and negative MNMBs during the northern winter months (between -2 and -33% during the months December to March). These deviations partly cancel each other out in MNMB for the whole evaluation period. For the RMSEs, (Fig. 5) maximum values also occur during the northern summer months with global average ranging between 11 and 16 ppb for June to September. The smallest errors appear during the northern hemisphere winter months (global average falling between 8 and 10 ppb for December and January). The correlation does not show a distinct seasonal behaviour (see Fig. 6).

The time series plots in Fig. 3 show that the seasonal cycle of O_3 mixing ratios with maximum concentrations during the summer months and minimum values occurring during winter times for European stations (e.g. Monte Cimone-MCI, Italy, Kosetice-KOS, Czech Republic, and Kovk- KOV, Slovenia), could well be reproduced by the model, although there is some overestimation in summer resulting mostly from observed minimum concentrations that are not captured correctly by the MACC_osuite, (Kosetice-KOS, Czech Republic, and Kovk- KOV, Slovenia).

The validation with EMEP surface ozone observations (described in section 2.2.2) in three different regions in Europe for the period 09/2009 to 12/2012 likewise confirms the behaviour of the model to overestimate O_3 mixing ratios during the warm period and underestimate O_3 concentrations during the cold period of the year (see Fig. 7). The positive bias (May-

November) is between -9 and 56% for northern Europe and Central Europe and between 8% and 48% for Southern Europe. Negative MNMBs appear, in accordance with GAW validation results, during the winter-spring period (December-April) ranging between -48 and -7% for EMEP stations in northern Europe (exception: December 2012 with 25%), between -1 and -39% in central Europe (exception: December 2012 with 31%), whereas in southern Europe, deviations are smaller and remain mostly positive (between -8 and 9%) in winter (exception: December 2012 with 37%). The different behaviour for December 2012 likely results from the limited availability of observations towards the end of the validation period. The separate evaluation of day and night-time O_3 mixing ratios (Fig. 8) shows that for northern Europe larger biases appear during night time. For central Europe and southern Europe night-time biases are larger during cold periods (December-April), whereas during warm periods (May–November) larger biases appear during day time.

3.2 Evaluation of Carbon Monoxide

The evaluation of the MACC_osuite with surface observations of 29 GAW stations (described in section 2.2.1) shows that over the whole period September 2009 to December 2012, CO mixing ratios could be reproduced with an average MNMB of -10%. The MNMBs for all stations range between -50 and +30%. Results are listed in Table 5, a selection of time series plots shows the results for stations in Europe, Asia and Canada in Fig. 9. MNMBs exceeding ± 30% appear for stations that are either located in or nearby cities and thus exposed to regional sources of contamination (Kosetice- KOS, Czech Republic) or are located in or near complex mountainous terrain (Rigi-RIG, Switzerland, BEO Moussala- BEO, Bulgaria) which is not resolved by the topography of the global model. RMSEs fall between 12 and 143 ppb (on average 48 ppb) for all stations during the validation period, but for only four stations (Rigi-RIG, Kosetice- KOS, Payerne-PAY, Switzerland and BEO Moussala-BEO, all located in Europe) do the RMSEs exceed 70 ppb. Correlation coefficients from the comparison with GAW station data calculated over the whole time period range between 0 and 0.8 (on average 0.4), with only four stations showing values smaller than 0.2 (Rigi-RIG, Moussala-BEO, East Trout Lake-ETL and Lac la Biche-LAC (the latter two located in Canada).

Considering the monthly MNMBs and RMSEs, it can be seen that during the northern hemisphere summer months, June to September, both are small (absolute differences less than 5%), see Fig. 10 and Fig. 11. Negative MNMBs (up to -35%) and larger RMSEs (up to 72 ppb) appear during the northern hemisphere winter months, November to March, when

14

anthropogenic emissions are at a highest, especially for the US, northern latitudes and Europe. Monthly correlation coefficients are between 0.1 and 0.5 and do not show a distinct seasonal behaviour (see Fig. 12), the low values of 0.1 during the period January 2011 to October 2011 result from the reading error in the fire emissions (see section 2.1.1). The generally only moderate correlation coefficient is related to mismatches in the strong short-term variability seen in both the model and the measurements.

The time series plots for stations in Europe, Asia and Canada in Fig. 9 demonstrate that the annual CO cycle could to a large degree be reproduced correctly by the model with maximum values occurring during the winter period and minimum values appearing during the summer season. However, the model shows a negative offset during the winter period. Seasonal air mass transport patterns that lead to regular annual re-occurring CO variations could be reproduced for GAW stations in East Asia: The time series plots for Yonagunijima- YON and Minamitorishima- MNM station, Japan (Fig. 9) show that the drop of CO, associated with the air mass change from continental to cleaner marine air masses after the onset of the monsoon season during the early summer months, is captured by the MACC_osuite. Deterioration in all scores is visible during December 2010 in the time series plots of several stations (e.g. Jungfraujoch-JFJ, and Sonnblick-SBL, Fig. 9). This is likely a result of changes in the processing of the L2 IASI data and a temporary blacklisting of IASI data (to avoid model failure) in the assimilation.

The comparison with MOPITT satellite CO total columns between October 2009 and June 2012 (described in section 2.2.3) shows a good qualitative agreement of spatial patterns and seasonality, see Table 6. The MNMBs for 8 regions are listed in Fig. 13 and range between 14% and -22%. The seasonality of the satellite observations is captured well by the MACC_osuite over Asia and Africa, with MNMBs between -6% and 9% (North Africa), -12% and 8% (South Africa), -11% and 12% (East Asia), and -3% and 14% (South Asia). The largest negative MNMBs appear during the winter periods, especially from December 2010 to May 2011 and from September 2011 to April 2012, for Alaska and Siberia and for the US and Europe (MNMBs up to -22%), which coincides with large differences between MOPITT and IASI satellite data (see Fig. 14). On the global scale the average difference between the IASI and MOPITT total columns is less than 10% (George et al., 2009), and there is a close agreement of MOPITT and IASI for S. Asia and Africa (see Fig. 14). However, larger differences between MOPITT and IASI data appear during the northern winter months over

Alaska, Siberia, Europe and the US, which result in lower CO concentrations in the model, due to the assimilation of IASI CO data in the MACC_osuite. The differences between MOPITT and IASI data can be mainly explained by the use of different a priori assumptions in the IASI and MOPITT retrieval algorithms (George et al., 2015 submitted). Indeed, the Fast Optimal Retrievals on Layers for IASI (FORLI) software (IASI) is using a single a priori CO profile (with an associated variance-covariance matrix) whereas the MOPITT retrieval algorithm is using a variable a priori, depending on time and location. George et al., 2015 (submitted) show that differences above Europe and the US in January and December (for a 5 year study) decrease by a factor of 2 when comparing IASI with a modified MOPITT product using the IASI single a priori. Between January 2011 and October 2011 there has also been a reading error in the fire emissions that contributes to larger MNMBs during this period (see section 2.1.1).

3.3 Evaluation of Tropospheric Nitrogen Dioxide

Figure 15 shows global maps of daily tropospheric NO_2 VCD averaged from September 2009 to March 2012. Overall, spatial distribution and magnitude of tropospheric NO_2 observed by SCIAMACHY are well reproduced by the model. This indicates that emission patterns and NO_x photochemistry are reasonably well represented by the model. However, the model underestimates tropospheric NO_2 VCDs over industrial areas in Europe, East China, Russia, and South East Africa compared to satellite data. This could imply that anthropogenic emissions from RETRO-REAS are underestimated in these regions, or that the lifetime in the model is too short. The model simulates larger NO_2 VCD maxima over Central Africa, which mainly originate from wild fires. It remains unclear if GFEDv2/GFAS fire emissions are too high here or if NO_2 fire plumes closer to the ground cannot be seen by the satellites due to light scattering by biomass burning aerosols (Leitao et al., 2010). In the northern hemisphere, background values of NO_2 VCD over the ocean are lower in the simulations than in the satellite data. The same is true for the South Atlantic Ocean to the west of Africa (see Fig.15). This might suggest a model underestimation of NO_2 export from continental sources or too rapid conversion of NO_2 into its reservoirs. However, as the NO_2 columns over the oceans are close to the uncertainties in the satellite data, care needs to be taken when interpreting these differences.

Time series of daily tropospheric NO_2 VCD averaged over different regions and corresponding monthly means are presented in Figs. 16 and 17, respectively. Time series of

the MNMB and RMSE are shown in Figs. 18 and 19, respectively. Table 7 summarizes the statistical values derived over the whole time period. High anthropogenic emissions occur over the United States, Europe, South Asia and East Asia compared to other regions on the globe (e.g., Richter et al., 2005). In principle, the MACC_osuite catches the pattern of satellite NO_2 VCD over these regions. However, the model tends to underestimate NO_2 VCDs throughout the whole time period investigated here. The negative bias is most pronounced over East Asia with a modelled mean NO_2 VCD for September 2009 to December 2012 of about 3.8 x 10^{15} molec cm^{-2} lower than that derived from satellite measurements (see Table 7).

Considering monthly values, the MACC_osuite strongly underestimates magnitude and seasonal variation of satellite NO_2 VCD over East Asia (MNMBs between about -40 % and -110 % and RMSE between 1 x 10^{15} molec cm^{-2} and 14 x 10^{15} molec cm^{-2} throughout the whole time period). A change in the modelled NO_2 values is apparent in July 2012 when the emission inventories changed and the agreement with the satellite data improved for South and East Asia but deteriorated for the US and Europe. This results in a drop of MNMBs (Fig. 18) for Europe and the US with values approaching around -70% by the end of 2012. Nevertheless, correlations between daily satellite and model data derived for the whole time period (see Table 7) are high for East Asia (0.8), South Asia (0.8), Europe (0.8), and lower, but still rather high, for the US (0.6).

The North African and South African regions are strongly affected by biomass burning (Schreier et al., 2013). Magnitude and seasonality of daily and monthly tropospheric NO_2 VCDs (Figs. 16 and 17, respectively) are rather well represented by the model, apart from January 2011 to October 2011, due to difficulties in reading fire emissions for this time period (see section 2.1.1). The latter results in large absolute values of the MNMB (Fig. 18) and large RMSEs (Fig. 19) between January 2011 and October 2011 compared to the rest of the time period. As for other regions investigated in this section, mean values of simulated daily tropospheric NO_2 VCDs over North Africa and South Africa between September 2009 and December 2012 tend to be lower than the corresponding satellite mean values (see Table 7). The correlation between daily model and satellite data over the whole time period is about 0.6 for South Africa and 0.5 for North Africa. It should be investigated in future studies, if this difference in model performance for the African regions is due to meteorology, chemistry or emissions.

4   Discussion

The validation of global O_3 mixing ratios with GAW observations at the surface levels showed that the MACC_osuite could generally reproduce the observed annual cycle of ozone mixing ratios. Model validation with surface data shows global average monthly MNMBs between -30% and 30% (GAW) and for Europe between -50% and 60% (EMEP). The bias between measured O_3 surface mixing ratios and the MACC_osuite is seasonally dependent, with an underestimation of the observed O_3 mixing ratios during the northern winter season and an overestimation during the summer months.

The validation of day-time versus night-time concentrations for Northern and Central Europe shows larger negative MNMBs in the winter months during night time than day time (Fig. 8), so that the negative bias in winter could be attributed to the simulation of vertical mixing at night, also described by Ordoñez (2010) and Schaap (2008), which remains a challenge in the model. The systematic underestimation of O_3 mixing ratios throughout the year for high latitude northern regions and Antarctica has its origin in an overestimation of the O_3 dry deposition velocities over ice. With the implementation of the new model cycle and MOZART model version, which includes updated velocity fields for the dry deposition of O_3, as described in Stein et al. (2013), the negative offset in the MACC_osuite model has been remedied for high latitude regions from July 2012 onwards (see the time series plots for the South Pole station- SPO and Neumayer- NEU in Fig. 3). The overestimation of O_3 mixing ratios for the northern hemisphere summer months is a well-known issue and has been described by various model validation studies (e.g., Brunner et al., 2003, Schaap et al., 2008, Ordoñez et al., 2010, Val Martin et al., 2014). Inadequate ozone precursor concentrations and aerosol induced radiative effects (photolysis) have been frequently identified as being the main factors. The time series plots in Fig. 3, however, demonstrate that the minimum concentrations in particular are not captured by the model during summer. Possible explanations include a general underestimation of NO titration which especially applies to stations with urban surroundings and strong sub-grid scale emissions (e.g. Tsukuba-TSU Fig. 3), including difficulties by the global model to resolve NO titration in urban plumes. It also seems likely that dry deposition at wet surfaces in combination with the large surface sink gradient due to nocturnal stability cannot be resolved with the model's vertical resolution. In regions such as Central and Southern Europe (Fig. 8) where day time biases exceed night time biases, the overestimation of O_3 might be related to an underestimation of day-time dry

1 deposition velocities: Val Martin et al., (2014) describe a reduction of the summertime O_3

2 model bias for surface ozone after the implementation of adjustments in stomatal resistances

3 in the MOZART model's dry deposition parameterization.

4 The MACC_osuite model realistically reproduces CO total columns over most of the

5 evaluated regions with monthly MNMBs falling between 10% and -20% (Table 6). There is a

6 close agreement of modelled CO total columns and satellite observations for Africa and South

7 Asia throughout the evaluation period. However, there is a negative offset compared to the

8 observational CO data over Europe and North America. The largest deviations occur during

9 the winter season when the observed CO concentrations are at a highest. The evaluation with

10 GAW surface CO data accordingly shows a wintertime negative bias of up to -35% at the

11 surface for stations in Europe and the US. A general underestimation of CO from global

12 models in the northern hemisphere has been described by various authors (e.g., Shindell et al.,

13 2006, Naik et al., 2013). According to Stein et al. (2014) this underestimation likely results

14 from a combination of errors in the dry deposition parameterization and certain limitations in

15 the current emission inventories. The latter include too low anthropogenic CO emissions from

16 traffic or other combustion processes and missing anthropogenic VOC emissions in the

17 inventories together with an insufficiently established seasonality in the emissions. An

18 additional reason for the apparent underestimation of emissions in MACCity may be an

19 exaggerated downward trend in the RCP8.5 (Representative Concentration Pathways)

20 scenario in North America and Europe between 2000 and 2010, as this scenario was used to

21 extrapolate the MACCity emissions from their bench mark year, i.e. 2000. For CO,

22 uncertainties in the evaluation also include the retrieved amount of CO total columns between

23 IASI and MOPITT. These vary with region, with IASI showing lower CO concentrations in

24 several regions (Alaska, Siberia, Europe and the US) during the northern winter months,

25 which possibly contribute to the deviations observed between the modelled data and MOPITT

26 satellite data, as only IASI data has been assimilated in the model. The differences can

27 primarily be explained by the use of different a priori assumptions in the IASI and MOPITT

28 retrieval algorithms (George et al., 2015 submitted). On a global scale however, the average

29 difference between the IASI and MOPITT total columns is less than 10% (George et al.,

30 2009). From July 2012 onwards, MOPITT CO total columns are also assimilated in the

31 MACC_osuite.

1   Modelled NO_2 total columns agree well with satellite observations over the United States,
2   South Asia and North Africa. However, there is also a negative offset for NO_2 over Europe
3   and East Asia. Again, the largest deviations are occurring during the winter season. The
4   quality of the emission inventory is even more crucial for short lived reactive species such as
5   NO_2, where model results depend to a large extent on emission inventories incorporated in the
6   simulations. This is highlighted by the deterioration of agreement between model results and
7   satellite data for the US in July 2012 when anthropogenic emissions were changed from
8   RETRO-REAS to MACCity. This change led to an increasing negative bias in NO_2 over
9   Europe and North America and to an improvement for South and East Asia (see Fig. 18). A
10 deterioration in MNMBs associated with the fire emissions is visible between January 2011
11 and October 2011 over regions with heavy fire activity (Africa and East Asia), and goes back
12 to a temporary error in the model regarding the reading of fire emissions (see Figs. 17 and
13 18). Particular challenges for an operational forecast system are regions with rapid changes in
14 emissions such as China, where inventories need to be extrapolated to obtain reasonable
15 trends. A large underestimation of NO_2 in China especially in winter has been reported for
16 other CTMs in previous publications (He et al., 2007, Itahashi et al., 2014). The latter has
17 been linked to an underestimation of NO_x and VOC emissions, unresolved seasonality in the
18 emissions and expected non-linearity of NO_x chemistry. The change in validation data sets
19 from SCIAMACHY to GOME-2 has shown to have negligible impact on the validation
20 results and conclusions.

21

5   Conclusion

23 The MACC_osuite is the global near-real-time MACC model analysis run for aerosol and
24 reactive gases. The model has been evaluated with surface observations and satellite data
25 concerning its ability to simulate reactive gases in the troposphere. Results showed that the
26 model proved capable of a realistic reproduction of the observed annual cycle for CO and O_3
27 mixing ratios at the surface, however, with seasonally dependent biases. For ozone, these
28 seasonal biases likely result from difficulties in the simulation of vertical mixing at night and
29 deficiencies in the model's dry deposition parameterization. For CO, a negative offset in the
30 model during the winter season is attributed to limitations in the emission inventories together
31 with an insufficiently established seasonality in the emissions.

CO and NO$_2$ total columns derived from satellite sensors could be reproduced over most of the evaluated regions, but showed a negative offset compared to the observational data over Europe and North America (CO) and over Europe and East Asia (NO$_2$). It has become clear, that that the emission inventories play a crucial role for the quality of model results and remain a challenge for near-real-time modeling, especially over regions with rapid changes in emissions.Inco nsistencies in the assimilated satellite data and fire emissions showed only a temporary impact on the quality of model results.

The MACC NRT system is constantly evolving. A promising step in model development is the on-line integration of modules for atmospheric chemistry in the IFS, currently being tested for implementation in the MACC_osuite. In contrast to the coupled model configuration as used in this paper, the on-line integration in the Composition IFS (C-IFS) provides major advantages; apart from an enhanced computational efficiency, C-IFS promises an optimization of the implementation of feedback processes between gas-phase/aerosol chemical processes and atmospheric composition and meteorology, which is expected to improve the modeling results for reactive gases. Additionally, C-IFS will be available in combination with different CTMs, (MOZART and TM5), which will help to explain whether deviations between model and observations go back to deficiencies in the chemistry scheme of a model.

21

Nacional de Meteorologia e Geofisica (INMG) (Cape Verde), National Air Pollution Monitoring Network (NABEL) (Federal Office for the Environment FOEN and Swiss Federal Laboratories for Materials Testing and Research EMPA), Japan Meteorological Agency (JMA), Alfred Wegener Institute, Umweltbundesamt (Austria), National Meteorological Service (Argentina), Umweltbundesamt (UBA, Germany). We thank the National Center for Atmospheric Research (NCAR) MOPITT science team and the NASA Langley Research Center, Atmospheric Science Data Center (ASDC), for producing and archiving the MOPITT CO product. IASI has been developed and built under the responsibility of the Centre National D'Etudes Spatiales (CNES, France). We are grateful to Juliette Hadji-Lazaro and the UBL/ LATMOS IASI team for establishing the IASI-MACC near real time processing chain. We wish to acknowledge that SCIAMACHY lv1 (level 1) radiances were provided to the Institute of Environmental Physics, University of Bremen by ESA through DLR/DFD.

References

Aas, W., Hjellbrekke, A.-G., Schaug, J.: Data quality 1998, quality assurance and field comparisons. Kjeller, Norwegian Institute for Air Research (EMEP/CCC-Report 6/2000), 2000.

Ashmore, M. R.: Assessing the future global impacts of ozone on vegetation. Plant Cell Environ. 28, 949–964, 2005.

Ballabrera-Poy, J., Kalnay, E. and Yang, S.: Data assimilation in a system with two scales—combining two initialization techniques. Tellus (2009), 61A, 539–549, doi:10.1111/j.1600-0870.2009.00400.x, 2009.

Bell M.L., R.D. Peng and F. Dominici: The exposure–response curve for O_3 and risk of mortality and the adequacy of current O_3 regulations. Environmental Health Perspectives, 114 (4), 2006.

Benedetti, A., Morcrette, J.-J., Boucher, O., Dethof, A., Engelen, R. J., Fisher, M., Flentje, H., Huneeus, N., Jones, L., Kaiser, J. W., Kinne, S., Mangold, A., Razinger, M., Simmons, A. J., Suttie, M., and the GEMS-AER team: Aerosol analysis and forecast in the European Centre for Medium-Range Weather Forecasts Integrated Forecast System: Data Assimilation. J. Geophys. Res., D13205, 114, doi:10.1029/2008JD011115, 2008.

Benedetti, A., Kaiser, J. W., and Morcrette J.-J:. [Global Climate] Aerosols [in "State of the Climate in 2010"]. B. Am.Meteor. Sci., 92(6):S65–S67, 2011.

1 Boersma, K.F., Eskes, H.J., Brinksma, E.J.: Error analysis for tropospheric NO2 retrieval
2 from space. J. Geophys. Res., 109, D4, doi:10.1029/2003JD003962, 2004.

3 Bovensmann, H., J. P. Burrows, M. Buchwitz, J. Frerick, S. Noël, V. V. Rozanov, K. V.
4 Chance, A. P. H. Goede: SCIAMACHY: Mission Objectives and Measurement Modes. J.
5 Atmos. Sci., 56, 127–150, 1999.

6 Brunner, D., Staehelin, J., Rogers, H. L., Köhler, M. O., Pyle, J. A., Hauglustaine, D.,
7 Jourdain, L., Berntsen T. K., Gauss, M., Isaksen, I. S. A., Meijer, E., van Velthoven, P.,
8 Pitari, G., Mancini, E., Grewe, V. and Sausen, R.: An evaluation of the performance of
9 chemistry transport models by comparison with research aircraft observations. Part 1:
10 Concepts and overall model performance. Atmos. Chem. Phys.., 3, 1609–1631,
11 doi:10.5194/acp-3-1609-2003, 2003.
12 Callies, J., Corpaccioli, E., Eisinger, M., Hahne, A., and Lefebvre, A.: GOME-2 Metop's
13 Second-Generation Sensor for Operational Ozone Monitoring, ESA Bull., 102, 28–36, 2000.

14 Cammas, J.-P., A. Gilles, S. Chabrillat, F. Daerden, N. Elguindi, J. Flemming, H. Flentje, C.

15 Deshler, T., J.L. Mercer, H.G.J. Smit, R. Stubi, G. Levrat, B.J. Johnson, S.J. Oltmans, R.
16 Kivi, A.M. Thompson, J. Witte, J. Davies, F.J. Schmidlin, G. Brothers, T. Sasaki
17 Atmospheric comparison of electrochemical cell ozonesondes from different maufacturers,
18 and with different cathode solution strengths: The Balloon Experiment on Standards for
19 Ozonsondes. J. Geophys. Res.113, D04307, doi:10.1029/2007JD008975, 2008.

20 Cape, J.N.: Surface ozone concentrations and ecosystem health: Past trends and a guide to
21 future projections. Science of the Total Environment Vol. 400, 257-269.,
22 doi:10.1016/j.scitotenv.2008.06.025, 2008.

23 Clarisse, L., R'Honi, Y., Coheur, P.-F., Hurtmans, D., and Clerbaux, C.: Thermal infrared
24 nadir observations of 24 atmospheric gases, Geophys. Res. Lett., 38, L10802,
25 doi:10.1029/2011GL047271, 2011.

26 Clerbaux, C., Boynard, A., Clarisse, L., George, M., Hadji-Lazaro, J., Herbin, H., Hurtmans,
27 D., Pommier, M., Razavi, A., Turquety, S., Wespes, C., and Coheur, P.-F.: Monitoring of
28 atmospheric composition using the thermal infrared IASI/MetOp sounder, Atmos. Chem.
29 Phys., 9, 6041–6054, doi:10.5194/acp-9-6041-2009, 2009.

30 Cooper, O. R., Parrish, D. D., Ziemke, J., Balashov, N. V., Cupeiro, M., Galbally, I. E., Gilge,
31 S., Horowitz, L., Jensen, N. R., Lamarque, J.-F., Naik, V., Oltmans, S. J., Schwab, J.,

Shindell, D. T., Thompson, A. M., Thouret, V., Wang, Y., Zbinden, R. M.: Global distribution and trends of tropospheric ozone: an observation-based review, Elem. Sci. Anth., 2,10 000029, doi:10.12952/journal.elementa.000029, 2014.

Cuevas, E., Camino, C., Benedetti, A., Basart, S., Terradellas, E., Baldasano, J.M., Morcrette, J.-J., Marticorena, B., Goloub, P., Mortier, A., Berjón, A., Hernández, Y., Gil-Ojeda, M., Schulz, M.: The MACC-II 2007-2008 Reanalysis: Atmospheric Dust Evaluation and Characterization over Northern Africa and Middle East, Atmos. Chem. Phys. 15, 3991–4024, doi:10.5194/acp-15-3991-2015, 2015.

Deeter, M. N., Emmons, L. K., Edwards, D. P., Gille, J. C., and Drummond, J. R.: Vertical resolution and information content of CO profiles retrieved by MOPITT, Geophys. Res. Lett., 31, L15112, doi:10.1029/2004GL020235, 2004.

Deeter, M. N., et al.: The MOPITT version 4 CO product: Algorithm enhancements, validation, and long-term stability, J. Geophys. Res., 115, D07306, doi:10.1029/2009JD013005, 2010.

Deeter, M. N., H. M. Worden, D. P. Edwards, J. C. Gille, D. Mao, and J. R. Drummond: MOPITT multispectral CO retrievals: Ori-gins and effects of geophysical radiance errors, J. Geophys. Res., 116, doi:10.1029/2011JD015703, 2011.

Deeter, M. N., Worden, H. M., Edwards, D. P., Gille, J. C., Andrews, A. E.: evaluation of MOPITT retrievals of lower-tropospheric carbon monoxide over the United States, J. Geophys. Res., 117, D13306, doi:10.1029/2012JD017553, 2012.

Deeter, M. N., Martínez-Alonso, S., Edwards, D. P., Emmons, L. K., Gille, J. C., Worden, H. M., Pittman, J. V., Daube, B. C., Wofsy, S. C.: Validation of MOPITT Version 5 thermal-infrared, near-infrared, and multispectral carbon monoxide profile retrievals for 2000–2011, J. Geophys. Res. Atmos., 118, 6710–6725, doi:10.1002/jgrd.50272, 2013.

De Wachter, E., Barret, B., Le Flochmoën, E., Pavelin, E., Matricardi, M., Clerbaux, C., Hadji-Lazaro, J., George, M., Hurtmans, D., Coheur, P.-F., Nedelec, P., and Cammas, J. P.: Retrieval of MetOp-A/IASI CO profiles and validation with MOZAIC data, Atmos. Meas. Tech., 5, 2843-2857, doi:10.5194/amt-5-2843-2012, 2012.

Drummond, J. R. and Mand, G. S.: The Measurements of Pollution in the Troposphere (MOPITT) Instrument: Overall Performance and Calibration Requirements. J. Atmos. Oceanic Technol., 13, 314–320, 1996.

Elguindi, N., Clark, H., Ordóñez, C., Thouret, V., Flemming, J., Stein, O., Huijnen, V., Moinat, P., Inness, A., Peuch, V.-H., Stohl, A., Turquety, S., Athier, G., Cammas, J.-P., and Schultz, M.: Current status of the ability of the GEMS/MACC models to reproduce the tropospheric CO vertical distribution as measured by MOZAIC, Geosci. Model Dev., 3, 501-518, doi:10.5194/gmd-3-501-2010, 2010.

Emmons, L. K., Edwards, D. P., Deeter, M. N., Gille, J. C., Campos, T., Nédélec, P., Novelli, P. and G. Sachse: Measurements of Pollution In The Troposphere (MOPITT) validation through 2006, Atmos. Chem. Phys., 9(5), 1795–1803, doi:10.5194/acp-9-1795-2009, 2009.

Engelen R. J., Serrar, S., Chevallier, F.: Four-dimensional data assimilation of atmospheric CO_2 using AIRS observations, J. Geophys. Res., 114, D03303, doi:10.1029/2008JD010739, 2009.

Flemming, J., and Inness, A., Volcanic sulfur dioxide plume forecasts based on UV satellite retrievals for the 2011 Grímsvötn and the 2010 Eyjafjallajökull eruption, Journal of Geophysical Research: Atmospheres118, 10172-10189, doi:10.1002/jgrd.50753, 2013.

Flemming, J., Inness, A., Flentje, H., Huijnen, V., Moinat, P., Schultz, M.G., Stein, O.: Coupling global chemistry transport models to ECMWF's integrated forecast system, Geosci. Model Dev., 2, 253-265, doi:10.5194/gmd-2-253-2009, 2009.

Forster, P., V. Ramaswamy, P. Artaxo, T. Berntsen, R. Betts, D.W. Fahey, J. Haywood, J. Lean, D.C. Lowe, G. Myhre, J. Nganga, R. Prinn, G. Raga, M. Schulz and R. Van Dorland: Changes in Atmospheric Constituents and in Radiative Forcing. In: Climate Change 2007: The Physical Science Basis. Contribution of Working Group I to the Fourth Assessment Report of the Intergovernmental Panel on Climate Change [S. Solomon, D. Qin, M. Manning, Z. Chen, M. Marquis, K.B. Averyt, M. Tignor and H.L. Miller (eds.)]. USA, 2007.

George, M., Clerbaux, C., Hurtmans, D., Turquety, S., Coheur, P.-F., Pommier, M., Hadji-Lazaro, J., Edwards, D. P., Worden, H., Luo, M., Rinsland, C., and McMillan,W.: Carbon monoxide distributions from the IASI/METOP mission: evaluation with other space-borne remote sensors, Atmos. Chem. Phys., 9, 8317–8330, doi:10.5194/acp-9-8317-2009, 2009.

George, M., Clerbaux, C., Bouarar, I., Coheur, P.-F., Deeter, M. N., Edwards, D. P., Francis, G., Gille, C., Hadji-Lazaro, J., Hurtmans, D., Inness, A., Mao, D., Worden H. M.: An

examination of the long-term CO records from MOPITT and IASI and comparison of retrieval methodology, Atmos. Meas. Tech. Discuss., submitted, 2015.

Gomez-Pelaez, A. J., Ramos, R., Gomez-Trueba, V., Novelli, P. C., and Campo-Hernandez, R.: A statistical approach to quantify uncertainty in carbon monoxide measurements at the Izaña global GAW station: 2008–2011, Atmos. Meas. Tech., 6, 787-799, doi:10.5194/amt-6-787-2013, 2013.

Granier, C., Huijnen, V., Inness, A., Jones, L., Katragkou E., Khokhar, F., Kins, L., Law, K., Lefever, K., Leitao, J., Melas, D., Moinat, P., Ordonez, C., Peuch, V.-H., Reich, G., Schultz, M., Stein, O., Thouret, V., Werner, T., Zerefos, C., GEMS GRG Comprehensive Validation Report. Available as project report at http://gems.ecmwf.int (last access: February 2015), 2009.

Granier, C., Bessagnet, B., Bond, T., D'Angiola, A., van der Gon, H. D., Frost, G. J., Heil, A., Kaiser, J. W., Kinne, S., Klimont, Z., Kloster, S., Lamarque, J.-F., Liousse, C., Masui, T., Meleux, F., Mieville, A., Ohara, T., Raut, J. C., Riahi, K., Schultz, M. G., Smith, S. J., Thompson, A., van Aardenne, J., van der Werf, G. R., and van Vuuren, D. P.: Evolution of anthropogenic and biomass burning emissions of air pollutants at global and regional scales during the 1980–2010 period, Climatic Change, 109, 163–190, doi:10.1007/s10584-011-0154-1, 2011.

Griffin, R.J., Chen, J., Carmody, K. and Vutukuru, S.: Contribution of gas phase oxidation of volatile organic compounds to atmospheric carbon monoxide levels in two areas of the united States. J. Geophys. Res., 11, D10S17, doi:10.1029/2006JD007602, 2007.

Guenther, A., Karl, T., Harley, P., Wiedinmyer, C., Palmer, P.I., and Geron, C.: Estimates of global terrestrial isoprene emissions using MEGAN (Model of Emissions of Gases and Aerosols from Nature), Atmos. Chem. Phys., 6, 3181-3210, doi:10.5194/acp-6-3181-2006, 2006.

He, Y, Uno, I., Wang, Z., Ohara, T., Sugimoto, N., Shimizu, A., Richter, A., Burrows, J. P.: Variations of the increasing trend of tropospheric NO_2 over central east China during the past decade, Atmospheric Environment, 41, 4865–4876, 2007.

Hilboll, A., Richter, A., and Burrows, J.P.: Long-term changes of tropospheric NO_2 over megacities derived from multiple satellite instruments, Atmos. Chem. Phys., 13, 4145-4169, doi:10.5194/acp-13-4145-2013, 2013a.

Hilboll, A., Richter, A., Rozanov, A., Hodnebrog, Ø., Heckel, A., Solberg, S., Stordal, F., and Burrows, J.P.,: Improvements to the retrieval of tropospheric NO_2 from Satellite – stratospheric correction using SCIAMACHY limb/nadir matching and comparison to Oslo CTM2 simulations. Atmos. Meas. Tech., 6, 565–584. doi:10.5194/amt-6-565-2013, 2013, 2013b.

Hollingsworth, A., Engelen, R.J., Benedetti, A., Dethof, A., Flemming, J., Kaiser, J.W., Simmons, A.J.: Toward a monitoring and forecasting system for atmospheric composition: The GEMS project, B.Am. Meteoro. Soc., 89, 1147–1164, doi:10.1175/2008BAMS2355.1, 2008.

Hudman, R.C., Murray, L.T., Jacob, D.J., Millet, D.B., Turquety, S., Wu, S., Blake, D.R., Goldstein, A.H., Holloway, J., Sachse, G.W.: Biogenic versus anthropogenic sources of CO over the United States. Geophys. Res. Let., 35, L04801, doi:10.1175/2007GL032393, 2008.

Huijnen, V., Williams, J., vanWeele, M., van Noije, T., Krol, M., Dentener, F., Segers, A., Houweling, S., Peters, W., de Laat, J., Boersma, F., Bergamaschi, P., van Velthoven, P., Le Sager, P., Eskes, H., Alkemade, F., Scheele, R., Nédélec, P., and Pätz, H.-W.: The global chemistry transport model TM5: description and evaluation of the tropospheric chemistry version 3.0, Geosci. Model Dev., 3, 445–473, doi:10.5194/gmd-3-445-2010, 2010.

Huijnen, V., Flemming, J., Kaiser, J. W., Inness, A., Leitao, J., Heil, A., Eskes, H. J., Schultz, M. G., Benedetti, A., Dufour, G., and Eremenko, M., Hindcast experiments of tropospheric composition during the summer 2010 fires over Western Russia, Atmos. Chem. Phys. 12, 4341-4364, doi:10.5194/acp-12-4341-2012, 2012.

Hurtmans, D., Coheur, P.-F., Wespes, C., Clarisse, L., Scharf, O., Clerbaux, C., Hadji-Lazaro, J., George, M., and Turquety, S.: FORLI radiative transfer and retrieval code for IASI. J Quant Spectrosc Radiat Transfer, 113, 1391–1408, doi:10.1016/j.jqsrt.2012.02.036, 2012.

Inness, A., Flemming, J., Suttie, M. and Jones, L.: GEMS data assimilation system for chemically reactive gases. ECMWF RD Tech Memo 587. Available from http://www.ecmwf.int. (last access: February 2015), 2009.

Inness, A., F. Baier, F., 2, Benedetti, A., Bouarar, I., Chabrillat, S., Clark, H., Clerbaux, C., Coheur, P., Engelen, R. J., Errera, Q., Flemming, J., George, M., Granier, C., Hadji-Lazaro, J., Huijnen, V., Hurtmans, D., Jones, L., Kaiser, J. W., Kapsomenakis, J., Lefever, K., Leitão J., Razinger, M., Richter, A., Schultz, M. G., Simmons, A. J., Suttie,M., Stein O., Thépaut J.-

N., Thouret,V., Vrekoussis, M., Zerefos, C, .al.: The MACC reanalysis: an 8 yr data set of atmospheric composition, Atmos. Chem. Phys. 13, 4073–4109, doi:10.5194/acp-13-4073-2013, 2013.

Inness, A., Blechschmidt, A.-M., Bouara, I., Chabrillat, S., Crepulja, M., Engelen, R. J., Eskes, H., Flemming, J., Gaudel, A., Hendrick, F., Huijnen, V., Jones, L., Kapsomenakis, J., Katragkou, E., Keppens, A., Langerock, B., de Mazière, M., Melas, D.,M. Parrington, V.H. Peuch, M. Razinger, A. Richter, M.G. Schultz, M. Suttie, V. Thouret, Vrekoussis, M., Wagner, A.,and Zerefos C.: Data assimilation of satellite retrieved ozone, carbon monoxide and nitrogen dioxide with ECMWF's Composition-IFS. Atmos. Chem. Phys., 15, 1–29, 2015.doi:10.5194/acp-15-1-2015.

Itahashi,S., Uno,I., Irie,H., Kurokawa,J.-I., and Ohara,T.: Regional modeling of tropospheric NO2 vertical column density over East Asia during the period 2000–2010: comparison with multisatellite observations, Atmos. Chem. Phys., 14, 3623-3635, doi:10.5194/acp-14-3623-2014, 2014.

Kaiser, J. W., Heil, A., Andreae, M. O., Benedetti, A., Chubarova, N., Jones, L., Morcrette, J.-J., Razinger, M., Schultz, M. G., Suttie, M., and van der Werf, G. R.: Biomass burning emissions estimated with a global fire assimilation system based on observed fire radiative power. Biogeosciences, 9, 527–554, doi:10.5194/bg-9-527-2012, 2012.

Kalnay, E., M. Kanamitsu, R. Kistler, W. Collins, D. Deaven, L. Gandin, M. Iredell, S. Saha, G. White, J. Woollen, Y. Zhu, M. Chelliah, W. Ebisuzaki, W. Higgins, J. Janowiak, K. C. Mo, C. Ropelewski, J. Wang, A. Leetmaa, R. Reynolds, R. Jenne, and D. Joseph: The NCEP/NCAR 40-Year Reanalysis Project. Bull. Amer. Meteor. Soc., 77, 437–471, doi:http://dx.doi.org/10.1175/1520-0477(1996)077<0437:TNYRP>2.0.CO;2, 1996.

Kalnay, E.: Atmospheric Modeling, Data Assimilation and Predictability. Cambridge University Press, 2003.

Kampa, M. and Castanas, E.: Human health effects of air pollution. Environmental PollutionVolume 151, Issue 2, 362–367, 2008.

Kerzenmacher, T., Dils, B., Kumps, N., Blumenstock, T., Clerbaux, C., Coheur, P.-F., Demoulin, P., García, O., George, M., Griffith, D. W. T., Hase, F., Hadji-Lazaro, J., Hurtmans, D., Jones, N., Mahieu, E., Notholt, J., Paton-Walsh, C., Raffalski, U., Ridder, T., Schneider, M., Servais, C., and De Mazi´ere, M.: Validation of IASI FORLI carbon monoxide

retrievals using FTIR data from NDACC, Atmos. Meas. Tech., 5, 2751–2761, doi:10.5194/amt-5-2751-2012, 2012.

Kinnison, D. E., Brasseur, G. P., Walters, S., Gracia, R. R., Marsh, D. R., Sassi, F., Harvey, V. L., Randall, C.E., Emmons, L., Lamarque, J. F., Hess, P., Orlando, J. J., Tie, X. X., Randel, W., Pan, L. L., Gettelman, A., Granier, C., Diehl, T., Niemeier, U. and Simmons, A. J.: Sensitivity of chemical tracers to meteorological parameters in the MOZART-3 chemical transport model. J. Geophys. Res, 112, D20302, doi:10.1029/2006JD007879, 2007.

Lefever, K., van der A, R., Baier, F., Christophe, Y., Errera, Q., Eskes, H., Flemming, J., Inness, A., Jones, L., Lambert, J.-C., Langerock, B., Schultz, M. G., Stein, O., Wagner, A., and Chabrillat, S.: Copernicus atmospheric service for stratospheric ozone: validation and intercomparison of four near real-time analyses, 2009–2012, Atmos. Chem. Phys. Discuss., 14, 12461-12523, doi:10.5194/acpd-14-12461-2014, 2014.

Leitão, J., Richter, A., Vrekoussis, M., Kokhanovsky, A., Zhang, Q. J., Beekmann, M., and Burrows, J. P.: On the improvement of NO_2 satellite retrievals – aerosol impact on the airmass factors, Atmos. Meas. Tech., 3, 475-493, doi:10.5194/amt-3-475-2010, 2010.

Leue, C., Wenig, M., Wagner, T., Platt, U. & Jähne, B. Quantitative analysis of NOx emissions from GOME satellite image sequences. J. Geophys. Res, 106, 5493–5505, 2001.

Massart, S., Agusti-Panareda, A., Aben, I., Butz, A., Chevallier, F., Crevosier, C., Engelen, R., Frankenberg, C., and Hasekamp, O.: Assimilation of atmospheric methane products into the MACC-II system: from SCIAMACHY to TANSO and IASI. Atmos. Chem. Phys., 14, 6139-6158, doi:10.5194/acp-14-6139-2014, 2014.

Mohnen, V.A., Goldstein, and Wang, W.-C.: Tropospheric Ozone and Climate Change, Air & Waste, 43:10, 1332-1334, doi:10.1080/1073161X.1993.10467207, 1993.

Morcrette, J.-J., Boucher, O., Jones, L., Salmond, D., Bechtold, P., Beljaars, A., Benedetti, A., Bonet, A., Kaiser, J.W., Razinger, M., Schulz, M., Serrar, S., Simmons, A.J., Sofiev, M., Suttie, M., Tompkins, A.M., Untch, A.: Aerosol analysis and forecast in the European Centre for Medium- Range Weather Forecasts Integrated Forecast System: forward modeling, J. Geophys. Res., 114, D06206, doi:10.1029/2008JD011235, 2009.

Naik, V., Voulgarakis, A., Fiore, M., Horowitz, L.W., Lamarque, J.-F., Lin, M., Prather, M. J., Young, P. J., Bergmann, D., Cameron-Smith, P. J., Cionni I., Collins W. J., Dalsøren, S. B., Doherty, R., Eyring V., Faluvegi, G., Folberth, G. A., Josse, B., Lee, Y. H., MacKenzie, I.

A., Nagashima,T., van Noije, T. P. C., Plummer, D. A., Righi, M., Rumbold, S. T., Skeie, R. D., Shindell, T., Stevenson, D. S., Strode, S., Sudo, K., Szopa, S., and Zeng, G. : Preindustrial to present-day changes in tropospheric hydroxyl radical and methane lifetime from the Atmospheric Chemistry and Climate Model Intercomparison Project (ACCMIP). Atmos. Chem. Phys., 13, 5277–5298, doi:10.5194/acp-13-5277-2013, 2013.

Novelli, P.C., Masarie, K.A. and Lang, P.M.: Distributions and recent changes of carbon monoxide in the lower troposphere, J. Geophys. Res., 103, 19015-19033, doi:10.1029/98JD01366, 1998.

Ordoñez, C., Elguindi, N., Huijnen, V., Flemming, J., inness, A., Flentje, H., Katragkou, E., Moinat, P., Peuch, V.-H., Segers, A., Thouret, V., Athier, G., van Weele, M., Zerefos, C.s., Cammas, J.-P., Schulz, M.G.: Global Model simulations of air pollution during the 2003 European heat wave. Atmos. Chem. Phys., 10, 789-815, doi:10.5194/acp-10-789-2010, 2010.

Park, R.J., Pickering, K.E., Allen, D. J : Global simulation of tropospheric ozone using the University of Maryland Chemical Transport Model (UMD-CTM): 1. model description and evaluation. J. Geophys. Res., 109, doi:101029/2003JD004266, 2004.

Penkett, S., Gilge, S., Plass-Duelmer, C. Galbally, I.: WMO/GAW Expert Workshop on Global Long-term Measurements of Nitrogen Oxides and Recommendations for GAW Nitrogen Oxides Network, WMO, Geneva, 2011.

Platt, U., and Stutz, J.: Differential Optical Absorption Spectroscopy. Physics of Earth and Space Environments. Berlin: Springer, http://www.springerlink.com/content/978-3-540-21193-8 (last access: February. 2015), 2008.

Richter, A., and Burrows, J.P.: "Tropospheric NO_2 from GOME Measurements." Advances in Space Research 29, no. 1, 1673–1683. doi:10.1016/S0273-1177(02)00100-X, 2002.

Richter, A., Burrows, J. P., Nüß, H., Granier, C, Niemeier, U.: Increase in tropospheric nitrogen dioxide over China observed from space, Nature, 437-132,doi:10.1038/nature04092, 2005.

Richter, A. Begoin, M., Hilboll, A., and Burrows, J. P.: An improved NO_2 retrieval for the GOME-2 satellite instrument, Atmos. Meas. Tech., 4, 1147-1159, doi:10.5194/amt-4-1147-2011, 2011.

Rodgers, C. D.: Inverse Methods for Atmospheric Sounding, Theory and Practice, World Scientific, Singapore, 2000.

Rozanov, A., Vladimir V., Rozanov, M., Buchwitz, A., Kokhanovsky, A. and Burrows, J.P.:. "SCIATRAN 2.0 - A New Radiative Transfer Model for Geophysical Applications in the 175-2400 Nm Spectral Region." Advances in Space Research 36, no. 5: 1015–1019. doi:10.1016/j.asr.2005.03.012, 2005.

Santer, B. D., Sausen, R., Wigley, T. M. L. , Boyle, J. S. , AchutaRao, K., Doutriaux, C.,. Hansen, J. E, Meehl, G. A. , Roeckner, E., Ruedy, R., Schmidt, G., Taylor, K. E.: Behavior of tropopause height and atmospheric temperature in models, reanalyses, and observations: Decadal changes, J. Geophys. Res., 108(D1), 4002, doi:10.1029/2002JD002258, 2003.

Schaap, M., Renske, M. A., Timmermans, M. R., Boersen, G. A. C., Builtjes, P. J. H.: The LOTOS–EUROS model: description, validation and latest developments, Int. J. Environ. Pollut., 32, No. 2, 270-290, 2008.

Schreier, S. F., Richter, A., Kaiser, J. W., and Burrows, J. P.: The empirical relationship between satellite-derived tropospheric NO2 and fire radiative power and possible implications for fire emission rates of NOx, Atmos. Chem. Phys., 14, 2447–2466, doi:10.5194/acp-14-2447-2014, 2014.

Schultz, M.G., Backman, L., Balkanski, Y., Bjoerndalsaeter, S., Brand, R., Burrows, J.P., Dalsoeren, S., de Vasconcelos, M., Grodtmann, B., Hauglustaine, D.A., Heil, A., Hoelzemann, J.J., Isaksen, I.S.A., Kaurola, J., Knorr, W., Ladstaetter-Weißenmayer, B., Mota, A., Oom, D., Pacyna, J., Panasiuk, D., Pereira, J.M.C., Pulles, T., Pyle, J., Rast, S., Richter, A., Savage, N., Schnadt, C., Schulz, M., Spessa, A., Staehelin, J., Sundet, J.K., Szopa, S., Thonicke, K., van het, Bolscher M., van Noije, T. , van Velthoven, P., Vik, A.F., Wittrock, F. (2007): REanalysis of the TROpospheric chemical composition over the past 40 years (RETRO) — A long-term global modeling study of tropospheric chemistry, Final Report Jülich/ Hamburg, Germany, published as report no. 48/2007 in the series „Reports on Earth System Science" of the Max Planck Institute for Meteorology, Hamburg, ISSN 1614-1199, 2007.

Seinfeld, J. H., and Pandis, S. N.: Atmospheric Chemistry and Physics: From Air Pollution to Climate Change, John Wiley, Hoboken, N. J., 2006.

1   Selin, N.E., Wu, S., Reilly, J. M., Paltsev, S., Prinn, R.G. and Webster, M.D.: Global health

2   and economic impacts of future ozone pollution. Environ. Res. Lett. 4, doi:10.1088/1748-

3   9326/4/4/044014, 2009.

4   Shindell, D. T., et al.: Multimodel simulations of carbon monoxide: Comparison with

5   observations and projected near-future changes, J. Geophys. Res., 111, D19306,

6   doi:10.1029/2006JD007100, 2006.

7   Sinnhuber, B.M., Weber, M., Amankwah, A. and Burrows, J.P.: "Total Ozone during the

8   Unusual Antarctic Winter of 2002." Geophysical Research Letters 30, no. 11, 1580–1584.

9   doi:10.1029/2002GL016798, 2003.

10 Sinnhuber, M., Burrows, J.P., Chipperfield, M., P., Jackman, C. H., Kallenrode, M.-B.,

11 Künzi, K.F., and Quack, M.: A Model Study of the Impact of Magnetic Field Structure on

12 Atmospheric Composition during Solar Proton Events., Geophys.. Res. Lett., 30, 1818–1821,

13 doi:10.1029/2003GL017265, 2003.

14 S. Sitch, S., Cox, P. M., Collins, W. J., Huntingford, C.: Indirect radiative forcing of climate

15 change through ozone effects on the land-carbon sink. Nature 448, 791-794,

16 doi:10.1038/nature06059, 2007.

17 Stein, O., Schultz, M. G., Flemming, J., Inness, A., Kaiser, J., Jones, L., Benedetti, A.,

18 Morcrette, J.-J.: MACC Global air quality services – Technical Documentation. MACC

19 project deliverable D_G-RG_3.8, available at:

20 www.gmes-atmosphere.eu/documents/deliverables/g-rg/ (last access: February 2015), 2011.

21 Stein, O., Flemming, J., Inness, A., Kaiser, J. W., and Schultz, M. G.: Global reactive gases

22 and reanalysis in the 5 MACC project, J. Integr. Environ. Sci.,

23 doi:10.1080/1943815X.2012.696545, 2012.

24 Stein, O., Huijnen, V., Flemming, J.: Model description of the IFS-MOZART and IFS-TM5

25 coupled systems. MACC-II project deliverable D_55.4, available at:

26 https://www.gmes-atmosphere.eu/documents/maccii/deliverables/grg/ (last access: February

27 2015), 2013.

28 Stein, O., Schultz, M. G., Bouarar, I., Clark, H., Huijnen, V., Gaudel, A., George, M., and

29 Clerbaux, C.: On the wintertime low bias of Northern Hemisphere carbon monoxide found in

30 10 global model simulations, Atmos. Chem. Phys., 14, 9295–9316, doi:10.5194/acp-14-9295-

2014, 2014.

Tørseth, K., Aas, W., Breivik, K., Fjæraa, A. M., Fiebig, M., Hjellbrekke, A. G., Lund Myhre, C., Solberg, S., and Yttri, K. E.: Introduction to the European Monitoring and Evaluation Programme (EMEP) and observed atmospheric composition change during 1972–2009, Atmos. Chem. Phys., 12, 5447-5481, doi:10.5194/acp-12-5447-2012, 2012.

Valcke, S., Redler, R.: OASIS4 User Guide (OASIS4_0_2). PRISM–Support Initiative, Technical Report No 4, available at: http://www.prism.enes.org/Publications/Reports/OASIS4_User_Guide_T4.pdf (last access: February 2015), 2006.

Val Martin, M., Heald, C.L., Arnold, S.R.: Coupling dry deposition to vegetation phenology in the Community Earth System Model: Implications for the simulation of surface O_3. Geophys Res. Lett., 41, 2988-2996, doi:10.1002/2014GL059651, 2014.

Van der Werf, G. R., Randerson, J. T., Giglio, L., Collatz, G. J., and Kasibhatla, P. S.: Interannual variability in global biomass burning emissions from 1997 to 2004. Atmos. Chem. Phys., 6(11):3423–3441, doi:10.5194/acp-6-3423-2006, 2006.

Velders, G. J. M., Granier, C., Portmann, R. W., Pfeilsticker, K., Wenig, M., Wagner, T., Platt, U., Richter, A., and Burrows, J. P.: Global tropospheric NO_2 column distributions: Comparing 3-D model calculations with GOME measurements, J. Geophys. Res., 106, 12643– 12660, 2001.

Wang, P., Stammes, P., van der A, R., Pinardi, G., and van Roozendael, M.: FRESCO+: An improved O_2 A-band cloud retrieval algorithm for tropospheric trace gas retrievals, Atmos. Chem. Phys., 8, 6565-6576, doi:10.5194/acp-8-6565-2008, 2008.

Winkler, H., Sinnhuber, M., Notholt, J., Kallenrode, M.B., Steinhilber, F., Vogt, J., Zieger, B., Glassmeier, K.H. and Stadelmann, A.: Modeling impacts of geomagnetic field variations on middle atmospheric ozone responses to solar proton events on long timescales, J. Geophys. Res. 113, D02302, doi:10.1029/2007JD008574, 2008.

WMO:WMO Global Atmosphere Watch (GAW) Strategic Plan: 2008 – 2015. World Meteorological Organization, Geneva, Switzerland, 2007.

WMO: Guidelines for the Measurement of Atmospheric Carbon Monoxide, GAW Report No. 192, World Meteorological Organization, Geneva, Switzerland, 2010.

1 WMO: 16th WMO/IAEA Meeting on Carbon Dioxide, Other greenhouse Gases and Related

2 Measurement Techniques (GGMT-2011), Geneva, 2012.

3 WMO : Guidelines for the Continuous Measurements of Ozone in the

4 Troposphere, GAW Report No. 209, World Meteorological Organization, Geneva,

5 Switzerland, 2013.

6 Worden, H. M., Deeter, M. N., Edwards, D. P., Gille, J. C., Drummond, J. R. and Nedelec, P.

7 P.: Observations of near-surface carbon monoxide from space using MOPITT multispectral

8 retrievals, J. Geophys. Res., 115, doi:10.1029/2010JD014242, 2010.

9 Worden, H. M., Deeter, M. N., Edwards, D. P., Gille, J., Drummond, J., Emmons, L. K.,

10 Francis, G., Martínez-Alonso, S.: 13 years of MOPITT operations: lessons from MOPITT

11 retrieval algorithm development, Ann. Geophys., 56,, doi:10.4401/ag-6330, 2014.

1   Table 1: List of assimilated data in the MACC_osuite

Instrument	Satellite	Provider	Version	Type	Status
MLS	AURA	NASA	V02	O_3 Profiles	20090901 - 20121231
OMI	AURA	NASA	V883	O_3 Total column	20090901 - 20121231
SBUV-2	NOAA	NOAA	V8	O_3 6 layer profiles	20090901 - 20121231
SCIAMACHY	Envisat	KNMI		O_3 total column	20090916 - 20120408
IASI	MetOp-A	LATMOS/ULB		CO Total column	20090901 - 20121231
MOPITT	TERRA	NCAR	V4	CO Total column	20120705 - 20121231
OMI	AURA	KNMI	DOMINO V2.0	NO_2 Tropospheric column	20120705 - 20121231
OMI	AURA	NASA	v003	SO_2 Tropospheric column	20120705 - 20121231
MODIS	AQUA / TERRA	NASA	Col. 5	Aerosol total optical depth	20090901 - 20121231

2

1

Table 2: Description of the set-up of the MACC_osuite between 9/2009 and 12/2012. Details

on the assimilated data are provided in Table 1. A description of the emissions is given in

section 2.1.1 in the text.

Model Cycle	CTM	Assimilated Data	Emissions
CY36R1	MOZART v3.0	O_3 (MLS, OMI, SBUV-2 SCIAMACHY), CO (IASI)	RETRO / REAS / GEIA / GFEDv2/GFAS
CY37R3	MOZART v3.5	O_3 (MLS, OMI, SBUV-2), CO (IASI, MOPITT), NO_2 (OMI), SO_2 (OMI)	MACCity / MEGAN / GFASv1.0 daily

5

1   Table 3: List of GAW and EMEP stations used in the evaluation (GAW listed by label, EMEP

2   listed by region: Northern Europe NE, Central Europe CE and Southern Europe SE).

Station	Label/Region	Programme	Lat	Lon	Alt [m a.s.l.]	Station	Label/Region	Programme	Lat	Lon	Alt [m a.s.l.]
Ähtäri II	**NE**	EMEP	62.58	24.18	180	Masenberg	**CE**	EMEP	47.35	15.88	1170
Alert	ALT	GAW	82.45	-62.52	210	Mauna Loa	MAU	GAW	19.54	-155.58	3397
Arrival Heights	ARH	GAW	-77.80	166.67	184	Minamitorishima	MNM	GAW	24.29	153.98	8
Aspvreten	**NE**	EMEP	58.80	17.38	20	Montandon	**CE**	EMEP	47.30	6.83	836
Assekrem	ASS	GAW	23.27	5.63	2710	Monte Cimone	MCI	GAW	44.18	10.70	2165
Aston Hill	**NE**	EMEP	52.50	-3.03	370	Monte Velho	**SE**	EMEP	38.08	-8.80	43
Auchencorth	**NE**	EMEP	55.79	-3.24	260	Montelibretti	**CE**	EMEP	42.10	12.63	48
Ayia Marina	**SE**	EMEP	35.04	33.06	532	Montfranc	**CE**	EMEP	45.80	2.07	810
Barcarrola	**SE**	EMEP	38.47	-6.92	393	Morvan	**CE**	EMEP	47.27	4.08	620
Baring Head	BAH	GAW	-41.41	174.87	85	Narberth	**NE**	EMEP	51.23	-4.70	160
Barrow	BAR	GAW	71.32	-156.60	11	Neuglobsow	NGW/**NE**	GAW/EMEP	53.17	13.03	62
BEO Moussala	BEO	GAW	42.18	23.59	2925	Neumayer	NEU	GAW	-70.65	-8.25	42
Birkenes	**NE**	EMEP	58.38	8.25	190	Niembro	**CE**	EMEP	43.44	-4.85	134
Bredkälen	**NE**	EMEP	63.85	15.33	404	Norra-Kvill	**NE**	EMEP	57.81	15.56	261
Bush	**NE**	EMEP	55.86	-3.21	180	O Saviñao	**CE**	EMEP	43.23	-7.70	506
Cabauw	**NE**	EMEP	51.97	4.92	60	Offagne	**CE**	EMEP	49.88	5.20	430
Cabo de Creus	**CE**	EMEP	42.32	3.32	23	Oulanka	**NE**	EMEP	66.32	29.40	310
Cairo	CAI	GAW	30.08	31.28	35	Pallas	**NE**	EMEP	68.00	24.15	340
Campisabalos	**CE**	EMEP	41.28	-3.14	1360	Payerne	PAY/**CE**	GAW/EMEP	46.81	6.94	510
Cape Grim	CAG	GAW	-40.68	144.68	94	Penausende	**CE**	EMEP	41.28	-5.86	985
Cape Point	CAP	GAW	-34.35	18.48	230	Peyrusse Vieille	**CE**	EMEP	43.62	0.18	200
Cape Verde	CVO	GAW	16.85	-24.87	10	Pic du Midi	PIC/**CE**	GAW/EMEP	42.94	0.14	2877
Charlton Mackrell	**NE**	EMEP	51.06	-2.68	54	Pillersdor	**CE**	EMEP	48.72	15.94	315
Chaumont	**CE**	EMEP	47.05	6.98	1130	Preila	**NE**	EMEP	55.35	21.07	5
Chibougamau	CHI	GAW	49.68	-74.34	393	Prestebakke	**NE**	EMEP	59.00	11.53	160
Chopok	**CE**	EMEP	48.93	19.58	2008	Puy de Dôme	PUY/**CE**	GAW/EMEP	45.77	2.95	1465
Concordia	CON	GAW	-75.10	123.33	3233	Ragged Point	RAG	GAW	13.17	-59.43	45
De Zilk	**NE**	EMEP	52.30	4.50	4	Rao	**NE**	EMEP	57.39	11.91	10
Diabla Gora	**NE**	EMEP	54.15	22.07	157	Revin	**CE**	EMEP	49.90	4.63	390
Dobele	DOB	GAW	56.37	23.19	42	Rigi	RIG/**CE**	GAW/EMEP	47.07	8.46	1030
Doñana	**SE**	EMEP	37.03	-6.33	5	Rojen Peak	**CE**	EMEP	41.70	24.74	1750
Donon	**CE**	EMEP	48.50	7.13	775	Rucava	RUC/**NE**	GAW/EMEP	56.10	21.10	18
Dunkelsteinerwald	**CE**	EMEP	48.37	15.55	320	Ryori	RYO	GAW	39.03	141.82	260
East Trout Lake	ETL	GAW	54.35	-104.98	492	Sable Island	SAB	GAW	43.93	-60.02	5
Egbert	EGB	GAW	44.23	-79.78	253	San Pablo de los Montes	**SE**	EMEP	39.55	-4.35	917
Eibergen	**NE**	EMEP	52.08	6.57	20	Sandve	**NE**	EMEP	59.20	5.20	15
Els Torms	**CE**	EMEP	41.40	0.72	470	Schauinsland	SCH/**CE**	GAW/EMEP	47.92	7.92	1205
Eskdalemuir	**NE**	EMEP	55.31	-3.20	243	Schmücke	**NE**	EMEP	50.65	10.77	937
Esrange	**NE**	EMEP	67.88	21.07	475	Sibton	**NE**	EMEP	52.29	1.46	46
Estevan Point	ESP	GAW	49.38	-126.55	39	Śnieżka	**NE**	EMEP	50.73	15.73	1603
Eupen	**NE**	EMEP	51.46	6.00	295	Sonnblick	SBL/**CE**	GAW/EMEP	47.05	12.96	3106

Station	Code	Network	Lat	Lon	Alt	Station	Code	Network	Lat	Lon	Alt
Everest - Pyramid	EVP	GAW	27.96	86.82	5079	South Pole	SPO	GAW	-89.98	-24.80	2810
Finokalia	**SE**	EMEP	35.32	25.67	250	Spitsbergen	**NE**	EMEP	78.90	11.88	474
Forsthof	**CE**	EMEP	48.10	15.91	581	St. Osyth	**NE**	EMEP	51.78	1.08	8
Fraserdale	FRA	GAW	49.88	-81.57	210	Stará Lesná	**CE**	EMEP	49.15	20.28	808
Gänserndorf	**CE**	EMEP	48.33	16.73	161	Starina	**CE**	EMEP	49.05	22.27	345
Gerlitzen	**CE**	EMEP	46.69	13.92	1895	Stixneusiedl	**CE**	EMEP	48.05	16.68	240
Graz Platte	**CE**	EMEP	47.11	15.47	651	Strath Vaich Dam	**NE**	EMEP	57.73	-4.77	270
Great Dun Fell	**NE**	EMEP	54.68	-2.45	847	Summit	SUM	GAW	72.58	-38.48	3238
Grebenzen	**CE**	EMEP	47.04	14.33	1648	Svratouch	**CE**	EMEP	49.73	16.05	737
Grimsoe	**NE**	EMEP	59.73	15.47	132	Syowa Station	SYO	GAW	-69.00	39.58	16
Harwell	**NE**	EMEP	51.57	-1.32	137	Tänikon	**CE**	EMEP	47.48	8.90	540
Haunsberg	**CE**	EMEP	47.97	13.02	730	Topolniky	**CE**	EMEP	47.96	17.86	113
Heidenreichstein	**CE**	EMEP	48.88	15.05	570	Trinidad Head	TRI	GAW	41.05	-124.15	120
High Muffles	**NE**	EMEP	54.33	-0.80	267	Tsukuba	TSU	GAW	36.05	140.13	25
Hurdal	**NE**	EMEP	60.37	11.08	300	Tudor Hill	TUD	GAW	32.27	-64.87	30
Illmitz	**CE**	EMEP	47.77	16.77	117	Tustervatn	**NE**	EMEP	65.83	13.92	439
Iskrba	ISK/**CE**	GAW/EMEP	45.56	14.86	520	Tutuila	TUT	GAW	-14.24	-170.57	42
Izaña (Tenerife)	IZO	GAW	28.30	-16.50	2367	Ushuaia	USH	GAW	-54.85	-68.32	18
Jarczew	**NE**	EMEP	51.82	21.98	180	Utö	**NE**	EMEP	59.78	21.38	7
Jungfraujoch	JFJ/**CE**	GAW/EMEP	46.55	7.99	3578	Vavihill	**NE**	EMEP	56.01	13.15	175
Karasjok	**NE**	EMEP	69.47	25.22	333	Vezin	**NE**	EMEP	50.50	4.99	160
Keldsnor	**NE**	EMEP	54.73	10.73	10	Vilsandi	**NE**	EMEP	58.38	21.82	6
Kollumerwaard	KOW/**NE**	GAW/EMEP	53.33	6.28	1	Vindeln	VIN/**NE**	GAW/EMEP	64.25	19.77	225
Košetice	KOS/**CE**	GAW/EMEP	49.58	15.08	534	Virolahti II	**NE**	EMEP	60.53	27.69	4
Kovk	KOV/**CE**	GAW/EMEP	46.12	15.11	600	Vorhegg	**CE**	EMEP	46.68	12.97	1020
K-puszta	**CE**	EMEP	46.97	19.58	125	Vredepeel	**NE**	EMEP	51.54	5.85	28
Krvavec	**CE**	EMEP	46.30	14.54	1740	Waldhof	WAL/**NE**	GAW/EMEP	52.80	10.77	74
La Coulonche	**CE**	EMEP	48.63	-0.45	309	Westerland	WES/**NE**	GAW/EMEP	54.93	8.32	12
La Tardière	**CE**	EMEP	46.65	-0.75	143	Weybourne	**NE**	EMEP	52.95	1.12	16
Lac La Biche	LAC	GAW	54.95	-112.45	540	Wicken Fen	**NE**	EMEP	52.30	-0.29	5
Ladybower Res.	**NE**	EMEP	53.40	-1.75	420	Yarner Wood	**NE**	EMEP	50.59	-3.71	119
Lahemaa	**NE**	EMEP	59.50	25.90	32	Yonagunijima	YON	GAW	24.47	123.02	30
Lauder	LAU	GAW	-45.03	169.67	370	Zarodnje	**CE**	EMEP	46.42	15.00	770
Le Casset	**CE**	EMEP	45.00	6.47	750	Zarra	**SE**	EMEP	39.09	-1.10	885
Leba	**NE**	EMEP	54.75	17.53	2	Zavodnje	ZAV	GAW	46.43	15.00	770
Lerwick	**NE**	EMEP	60.13	-1.18	85	Zillertaler Alpen	**CE**	EMEP	47.14	11.87	1970
Lille Valby	**NE**	EMEP	55.69	12.13	10	Zingst	ZIN/**NE**	GAW/EMEP	54.43	12.73	1
Lough Navar	**NE**	EMEP	54.44	-7.87	126	Zoebelboden	**CE**	EMEP	47.83	14.44	899
Lullington Heath	**NE**	EMEP	50.79	0.17	120	Zoseni	ZOS/**NE**	GAW/EMEP	57.13	25.90	188
Mace Head	**NE**	EMEP	53.17	-9.50	15	Zugspitze	SFH	GAW	47.42	10.98	2656
Market Harborough	**NE**	EMEP	52.55	-0.77	145						

1

2

1   Table 4: Modified normalized mean bias (MNMB) [%], correlation coefficient (R), and root

2   mean square error (RMSE) [ppb] derived from the evaluation of the MACC_osuite with

3   Global Atmosphere Watch (GAW) O_3 surface observations during the period 09/2009 to

4   12/2012.

Station	ARH	ASS	BAH	BAR	BEO	CAI	CAG	CAP	CVO	CON	DOB	EVP	ISK	IZO	JFJ	KOW	KOS
MNMB	-39.8	-6.3	-8.6	-35.1	-21.4	70.1	-12.7	13.7	15.2	-81.6	6.3	18.4	67.2	10.4	1.9	5.8	-5.9
R	0.6	0.7	0.5	0.3	0.4	-0.1	0.4	0.6	0.6	0.3	0.3	0.7	0.1	0.5	0.7	0.6	0.6
RMSE	10.6	6.5	8.0	13.8	20.4	29.2	8.9	7.6	8.0	17.2	14.3	12.0	34.5	10.8	7.4	12.0	16.3

5

Station	KOV	KRV	LAU	MAU	MNM	MCI	NGW	NEU	PAY	PIC	PUY	RAG	RIG	RUC	RYO	SCH	SBL
MNMB	21.2	9.5	-5.5	13.7	38.6	2.3	-11.4	-45.2	-28.8	5.5	12.8	38.6	-80.3	-0.1	10.5	8.5	8.1
R	0.6	0.6	0.5	0.6	0.8	0.7	0.5	0.5	0.7	0.6	0.6	0.6	0.3	0.3	0.1	0.7	0.6
RMSE	19.5	11.1	9.0	11.5	13.0	8.2	14.3	11.4	15.6	7.7	10.6	10.6	28.4	15.0	14.4	12.2	9.3

6

Station	SFH	SPO	SUM	SYO	TRI	TSU	TUD	TUT	USH	VIN	WAL	WES	YON	ZAV	ZIN	ZOS
MNMB	10.1	-70.6	-24.4	-31.2	3.2	55.1	45.3	40.2	-7.0	4.6	-18.0	-12.3	22.0	19.7	-17.5	22.3
R	0.6	0.4	0.5	0.7	0.3	0.0	0.5	0.8	0.5	0.4	0.6	0.6	0.7	0.6	0.4	0.2
RMSE	9.3	16.3	11.7	8.9	13.3	27.6	18.2	8.0	7.6	11.2	13.6	11.6	13.6	18.6	13.9	17.0

7

1   Table 5: Modified normalized mean bias (MNMB) [%], correlation coefficient (R), and root

2   mean square error (RMSE) [ppb] derived from the evaluation of the MACC_osuite with

3   Global Atmospheric Watch (GAW) CO surface observations during the period 09/2009 to

4   12/2012.

Station	ALT	BEO	CAP	CHI	CVO	EGB	ESP	ETL	FRA	IZO	JFJ	KOS	KOW	KRV	LAC	MCI	MNM
MNMB	-6.9	-36.1	29.7	-7.3	-0.6	4.5	-1.7	-19.9	-12.0	-6.8	-15.1	-50.1	-5.9	-30.4	-24.2	-19.0	6.4
R	0.5	0.0	0.6	0.4	0.7	0.3	0.5	0.1	0.3	0.7	0.6	0.2	0.4	0.4	0.0	0.6	0.8
RMSE	23.4	90.3	20.4	31.1	14.2	60.1	25.7	53.9	35.9	15.3	25.8	131.1	70.1	49.1	58.5	32.0	22.0

5

Station	NGW	PAY	PIC	PUY	RIG	RYO	SAB	SBL	SCH	SFH	USH	YON
MNMB	-1.7	-7.3	-9.3	-10.4	28.2	-4.8	-8.1	-25.1	-15.8	-25.7	-9.1	-1.6
R	0.4	0.3	0.7	0.6	0.0	0.4	0.4	0.5	0.5	0.4	0.6	0.7
RMSE	61.6	99.2	18.4	30.6	143.5	44.5	31.6	36.8	39.8	45.0	12.3	62.3

6

1 Table 6: Modified normalized mean bias (MNMB) [%] derived from CO satellite

2 observations (MOPITT) and the MACC_osuite simulations of CO total columns from

3 10/2009 until 06/2012 averaged over different regions.

	Oct 09	Nov 09	Dec 09	Jan 10	Feb 10	Mar 10	Apr 10	May 10	Jun 10	Jul 10	Aug 10
Europe	4.17	1.35	-7.02	-7.17	-7.84	-8.56	-5.20	-2.15	-2.96	0.75	-2.88
Alaska	0.31	-3.16	-6.71	-8.85	-6.39	-3.13	-4.49	-3.85	-8.69	-6.18	-3.94
Siberia	2.02	1.62	-1.44	-2.75	-1.36	-2.27	-3.58	-2.93	-5.30	4.21	-8.43
N. Africa	6.53	9.17	5.82	7.05	3.45	-2.96	-3.53	-1.75	-3.40	-1.21	-3.58
S. Africa	-12.45	-9.44	3.10	6.53	8.27	6.63	3.57	2.33	7.34	0.57	-2.75
S. Asia	9.20	13.73	6.95	6.41	6.69	1.12	3.18	1.26	-3.01	1.98	2.15
E. Asia	8.04	12.33	-5.86	-9.18	-6.64	-4.49	-5.12	-5.61	-7.72	-4.34	-2.80
US	9.73	6.71	-5.42	-7.75	-10.88	-6.26	-3.80	-2.04	1.58	2.54	2.98
	Sep 10	**Oct 10**	**Nov 10**	**Dec 10**	**Jan 11**	**Feb 11**	**Mar 11**	**Apr 11**	**May 11**	**Jun 11**	**Jul 11**
Europe	-1.97	-0.92	-2.94	-7.78	-15.41	-17.22	-18.78	-17.34	-13.34	-6.62	-3.91
Alaska	-5.00	-1.89	-4.87	-7.51	-14.54	-9.90	-9.29	-12.54	-11.95	-10.04	-4.73
Siberia	-2.94	-1.93	-1.73	-3.02	-7.71	-7.78	-12.09	-21.99	-17.23	-11.59	-4.97
N. Africa	-1.22	3.33	5.98	7.03	-0.53	4.31	2.66	1.37	4.23	4.71	4.37
S. Africa	-5.13	2.84	7.39	4.37	1.41	3.39	3.80	0.99	5.71	3.45	-2.75
S. Asia	5.05	6.72	9.63	10.30	2.19	2.91	1.48	-1.76	1.68	1.62	2.90
E. Asia	6.13	6.93	2.44	3.23	-11.25	-9.18	-9.63	-8.58	-4.73	-1.62	5.00
US	0.08	-0.71	1.20	-8.06	-18.30	-16.98	-14.33	-13.52	-8.10	-4.72	-0.64
	Aug 11	**Sep 11**	**Oct 11**	**Nov 11**	**Dec 11**	**Jan 12**	**Feb 12**	**Mar 12**	**Apr 12**	**May 12**	**Jun 12**
Europe	-2.57	-7.28	-10.80	-11.85	-14.79	-13.50	-14.16	-15.30	-11.49	-7.00	-3.65
Alaska	-5.69	-11.86	-18.05	-14.33	-12.29	-11.50	-11.24	-11.92	-9.42	-8.71	-4.74
Siberia	-6.05	-15.16	-16.50	-10.32	-11.59	-10.15	-8.45	-13.14	-12.18	-11.08	-4.45
N. Africa	6.15	5.35	6.27	-0.93	3.37	2.04	1.11	-5.90	-3.40	-3.59	-0.95
S. Africa	-6.70	-4.43	-0.58	3.64	4.66	4.25	2.91	0.91	3.41	1.33	-1.23
S. Asia	3.80	2.27	4.24	4.76	7.00	3.24	1.72	-1.23	-0.90	0.49	-0.61
E. Asia	3.05	1.60	-2.60	-2.48	-5.15	-5.56	-4.63	-0.85	-0.36	-2.63	0.68
US	-1.17	-2.40	-4.23	-6.14	-10.84	-13.30	-14.87	-9.19	-6.94	-2.88	-2.55

4

1   Table 7: Statistics derived from satellite observations (SCIAMACHY from 09/2009 until

2   03/2012, GOME-2 from 04/2012 to 12/2012) and the MACC_osuite simulations of daily

3   tropospheric NO_2 VCD [10^{15} molec cm^{-2}] averaged over different regions for September 2009

4   to December 2012.

Region	United States	Europe	South Asia	East Asia	South Africa	North Africa
Model mean NO_2 VCD [10^{15} molec cm²]	2.6	2.1	1.0	2.4	0.8	0.9
Satellite mean NO_2 VCD [10^{15} molec cm²]	3.1	3.6	1.2	6.2	1.1	0.9
Modified normalized mean bias (MNMB) [%]	-17.3	-49.0	-13.4	-70.7	-36.8	-0.4
Root mean square error (RMSE) [10^{15} molec cm²]	1.2	2.0	0.3	6.0	0.5	0.3
Correlation coefficient (R) [dimensionless]	0.6	0.8	0.8	0.8	0.6	0.5

5

1

2
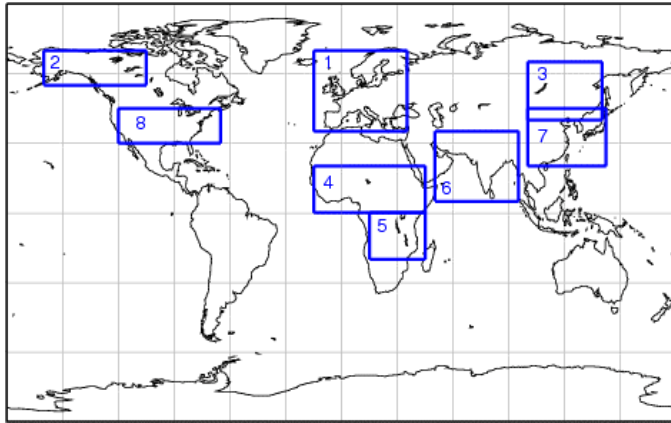
Figure 1: Regions used for regional data-stratification in the troposphere for the comparison with satellite data. The following regions are defined: **1** Europe (15W– 35E, 35N–70N), **2** Alaska (150W–105W, 55N–70N), **3** Siberia (100E–140E, 40N–65N), **4** North Africa (15W–45E, 0N–20N), **5** South Africa (15E–45E, 20S–0S), **6** South Asia (50E–95E, 5N–35N), **7** East Asia (100E–142E, 20N–45N), **8** United States (120W–65W, 30N–45N).
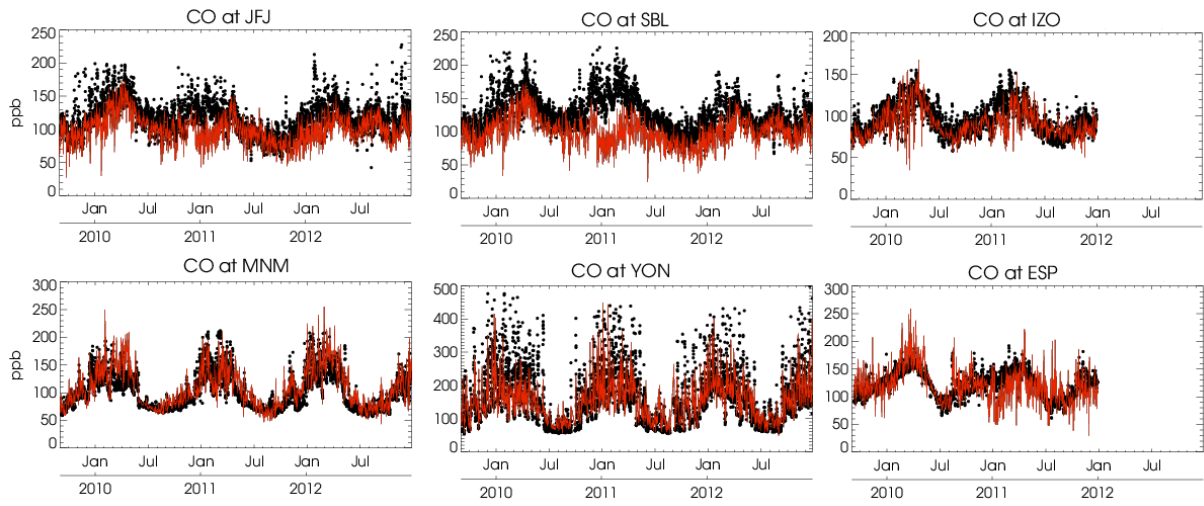
1

2

3   Figure 2: Modified normalized mean biases (MNMBs) [%] derived from the evaluation of the

4   MACC_osuite with GAW O$_3$ surface observations during the period 09/2009 to 12/2012

5   globally (top), and for Europe (below). Blue colours represent large negative values;

6   red/brown colours represent large positive values.
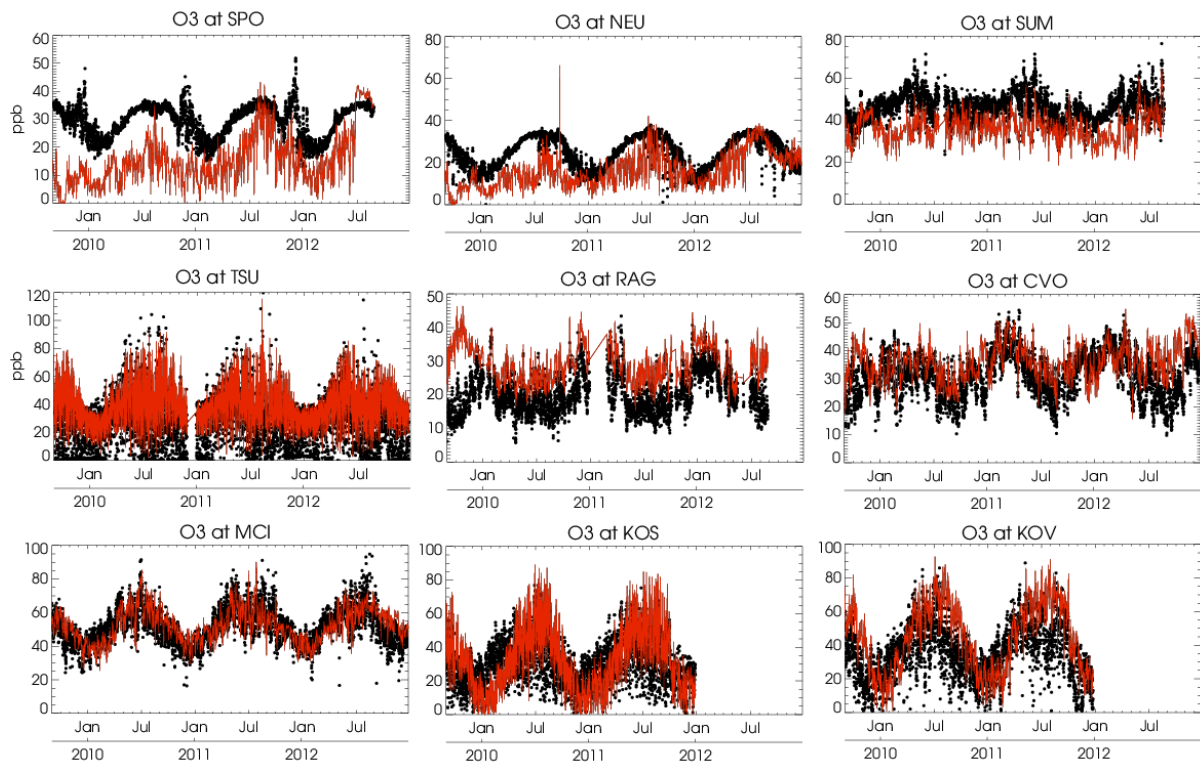
Figure 3: Time series plots of the MACC_osuite 6-hourly O_3 mixing ratios (red) and GAW surface observations (black) for South Pole-SPO (Antarctica), Neumayer-NEU (Antarctica), Summit-SUM (Denmark), Tsukuba-TSU (Japan), Ragged Point-RAG, (Barbados), Cape Verde Observatory-CVO (Cape Verde), Monte Cimone-MCI (Italy), Kosetice-KOS (Czech Republic), Kovk- KOV(Slovenia) during the period 09/2009 to 12/2012. Unit: ppb
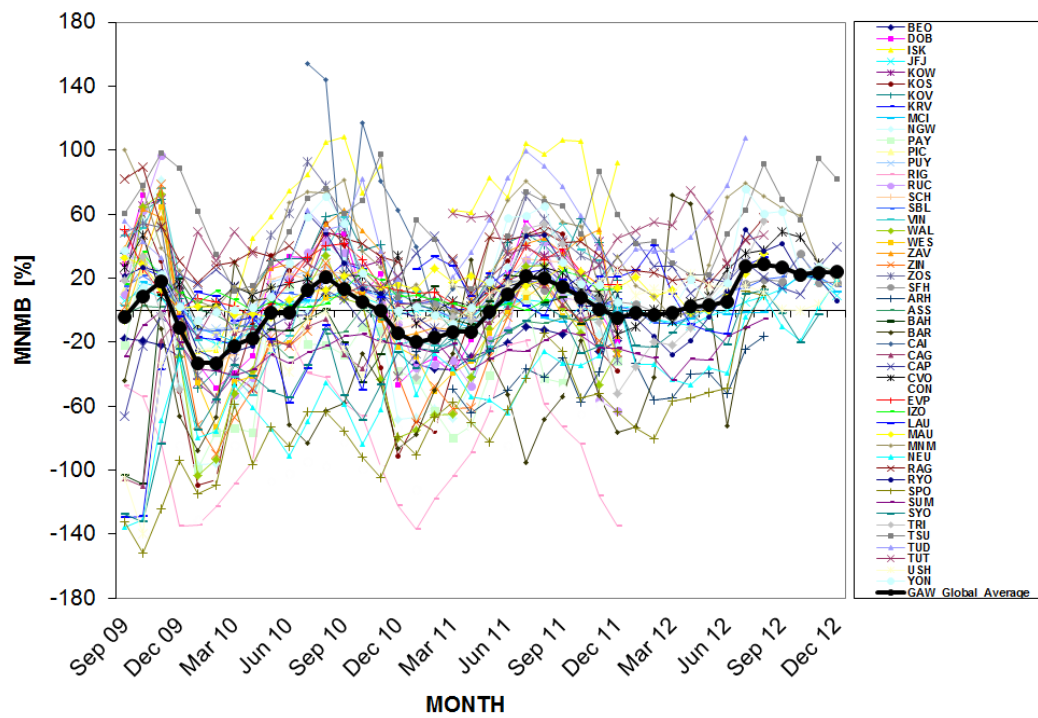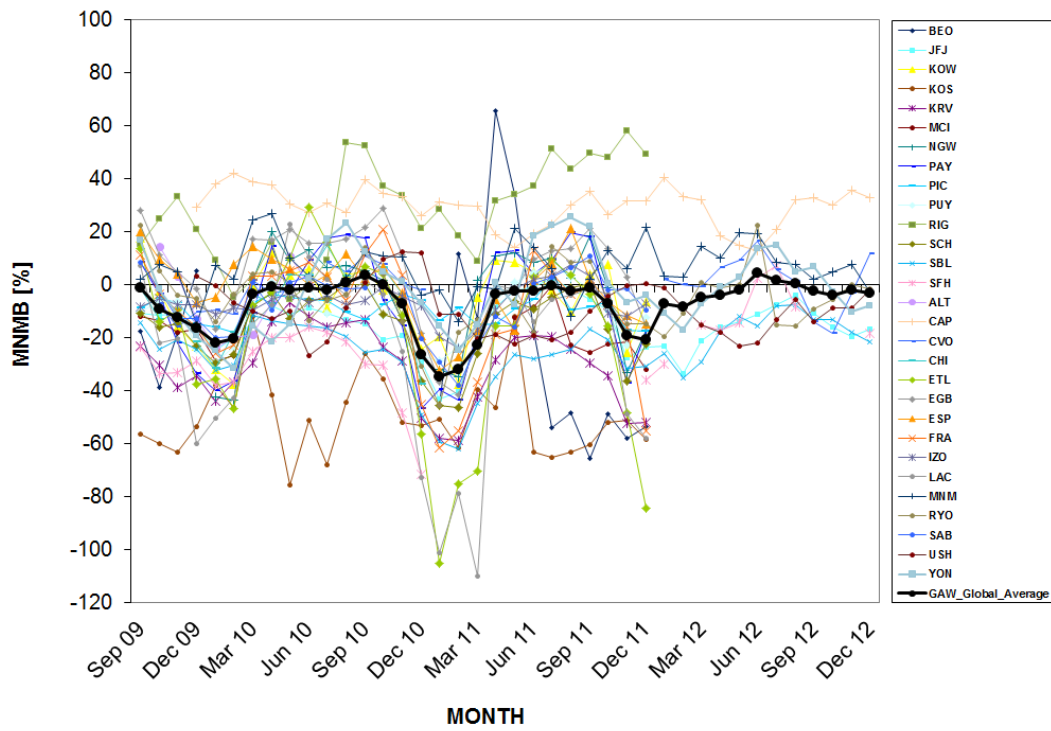
1

2 Figure 4: Modified normalized mean bias (MNMB) in % derived from the evaluation of the

3 MACC_osuite with GAW O$_3$ surface observations during the period September 2009 to

4 December 2012 (black line: global average of 50 GAW stations. Multi-coloured lines:

5 individual station results, see legend to the right).
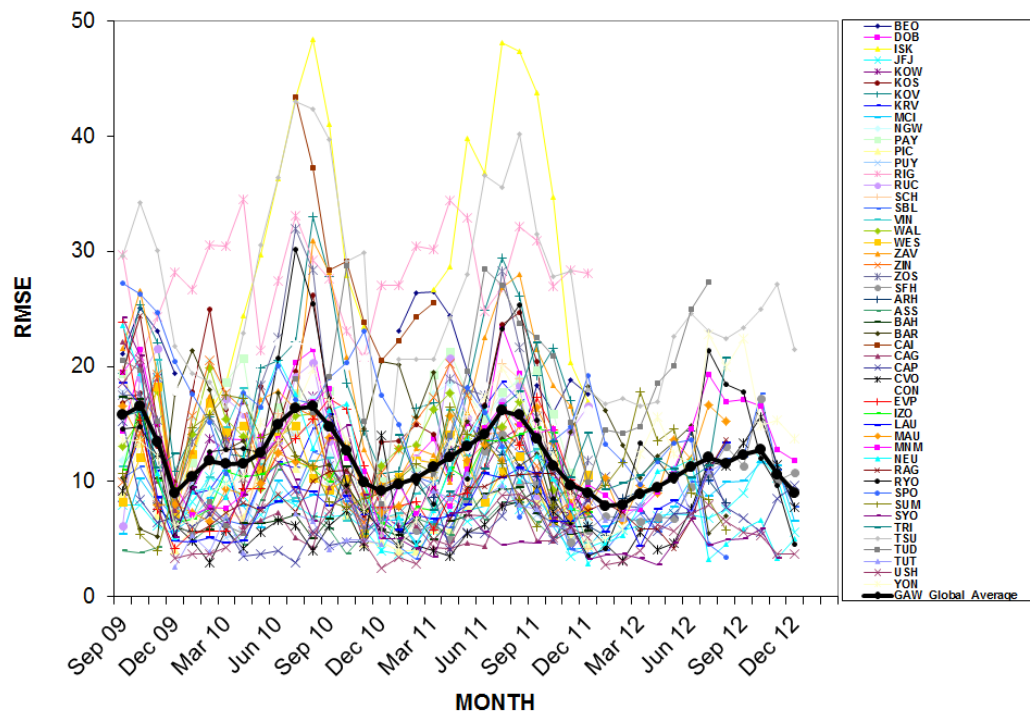
Figure 5: Root mean square error (RMSE) in ppb derived from the evaluation of the MACC_osuite with GAW O$_3$ surface observations during the period September 2009 to December 2012 (black line: global average of 50 GAW stations. Multi-coloured lines: individual station results, see legend to the right).
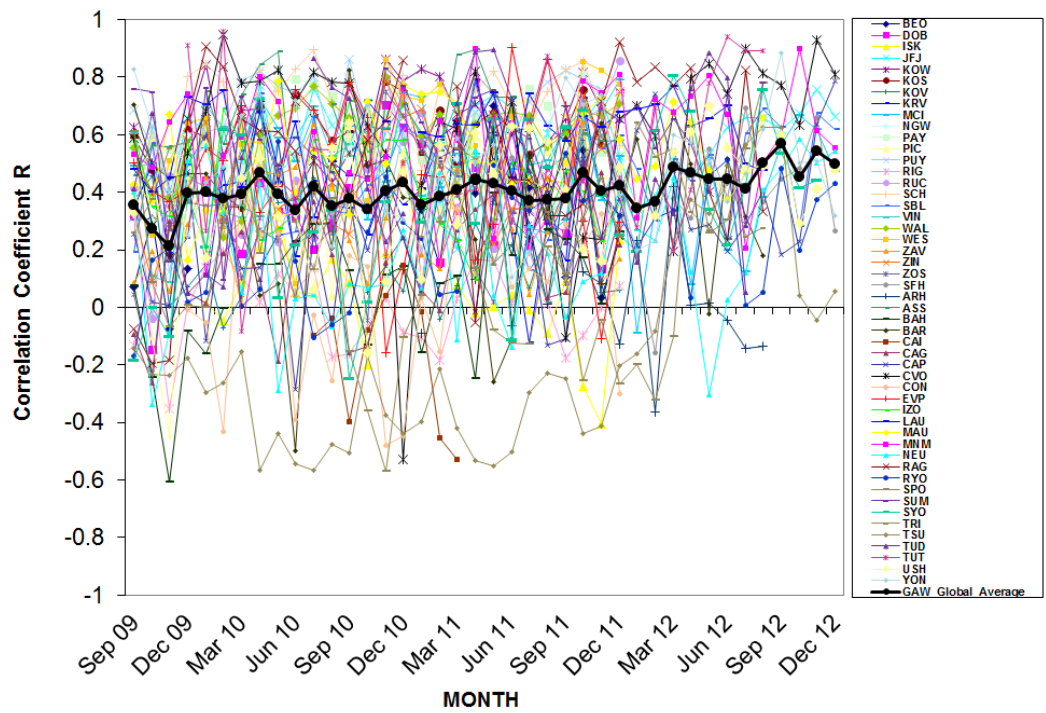
1

2   Figure 6: Correlation coefficient (R), derived from the evaluation of the MACC_osuite with

3   GAW O_3 surface observations during the period September 2009 to December 2012 (black

4   line: global average of 50 GAW stations. Multi-coloured lines: individual station results, see
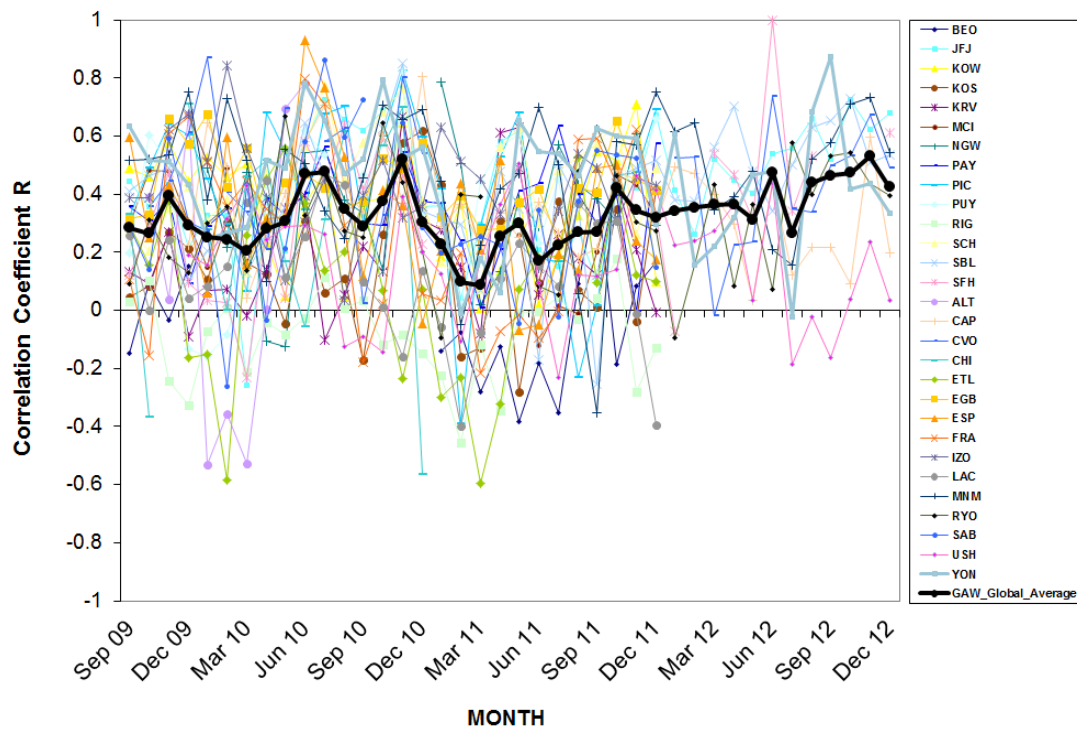
5   legend to the right).
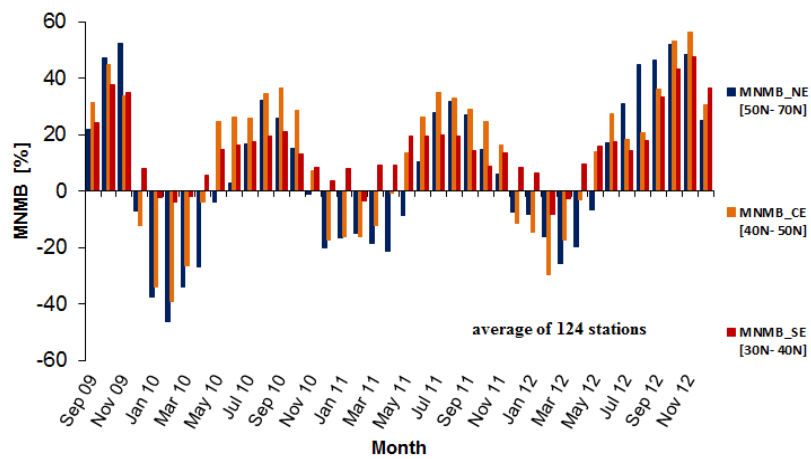
1

2   Figure 7: Modified normalized mean biases (MNMBs) derived from the evaluation of the

3   MACC_osuite with EMEP O$_3$ surface observations in three different parts in Europe (blue:

4   Northern Europe, orange: Central Europe, red: Southern Europe) during the period September

5   2009 to December 2012.
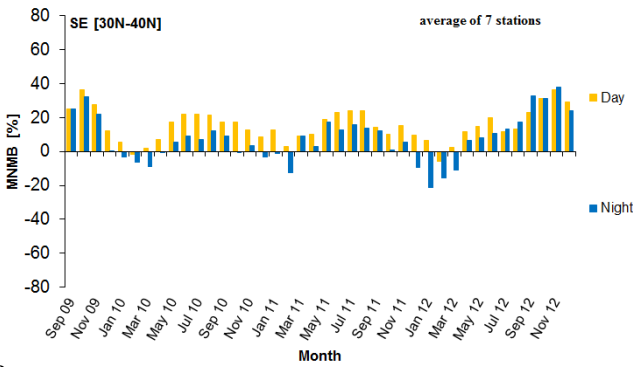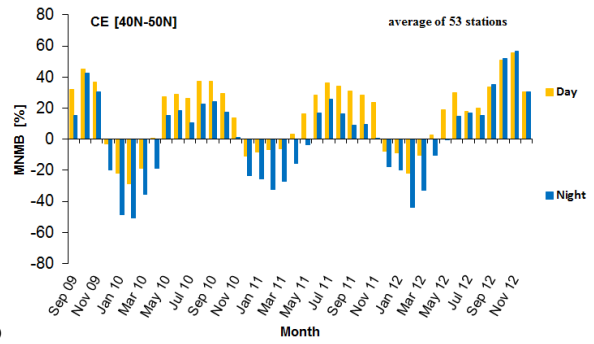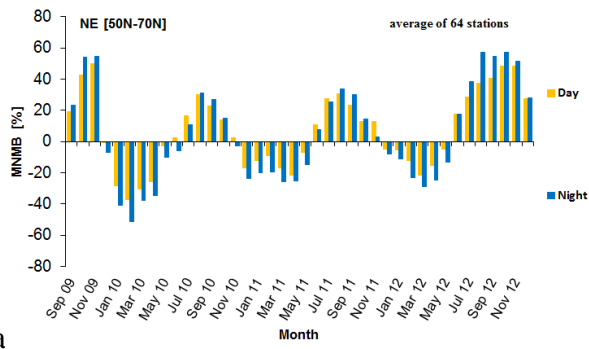
1   a   b

2   c

3   Figure 8: Modified normalized mean biases (MNMBs) derived from the evaluation of the

4   MACC_osuite with EMEP O_3 surface observations during day-time (yellow color), and night-

5   time (blue color) over northern Europe (a), central Europe (b) and southern Europe (c) during

6   the period September 2009 to December 2012.

Figure 9: Time series plots of the MACC_osuite 6-hourly CO mixing ratios (red) and GAW surface observations (black) for Jungfraujoch- JFJ (Switzerland), Sonnblick- SBL (Austria), Izana Observatory- IZO (Tenerife), Minamitorishima- MNM (Japan), Yonagunijima- YON (Japan), Estevan Point- EVP (Canada) during the period 09/2009 to 12/2012. Unit: ppb.

1

2   **MONTH**

3   Figure 10: Modified normalized mean bias (MNMB) in % derived from the evaluation of the

4   MACC_osuite with GAW CO surface observations over the period September 2009 to

5   December 2012 (black line: global average of 29 GAW stations. Multi-coloured lines:

6   individual station results, see legend to the right).
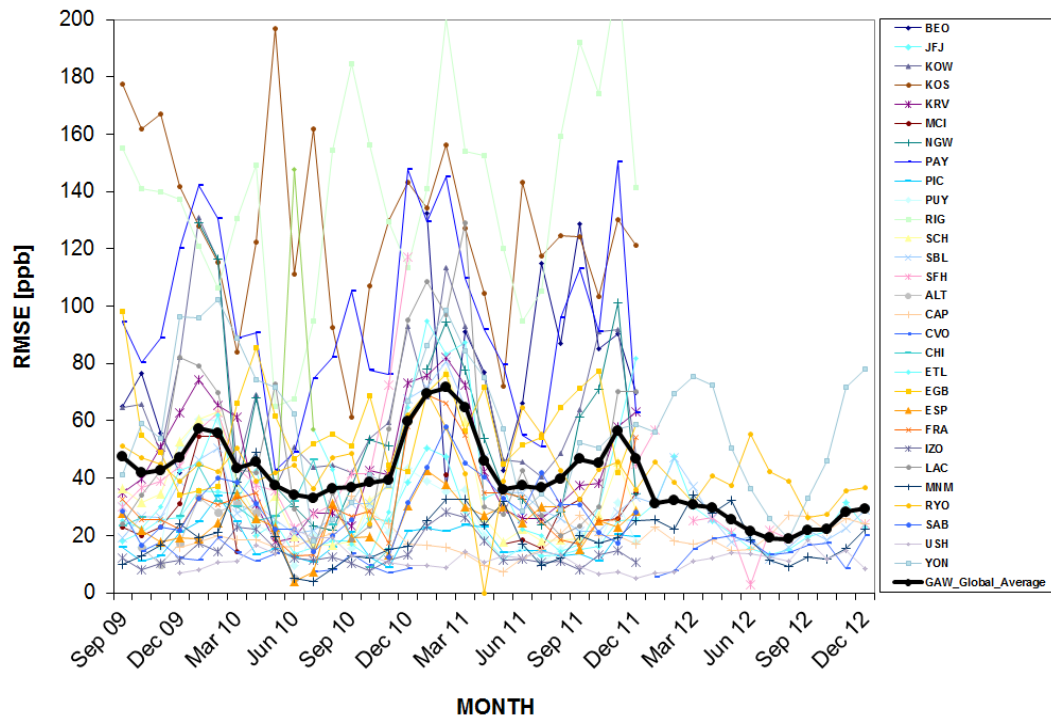
1

2 Figure 11: Root mean square error (RMSE) in ppb derived from the evaluation of the

3 MACC_osuite with GAW CO surface observations over the period September 2009 to

4 December 2012 (black line: global average of 29 GAW stations multi-coloured lines:

5 individual station results, see legend to the right).

1

2 Figure 12: Correlation coefficient (R), derived from the evaluation of the MACC_osuite with

3 GAW CO surface observations over the period September 2009 to December 2012 (black

4 line: global average of 29 GAW stations. Multi-coloured lines: individual station results, see

5 legend to the right).

6
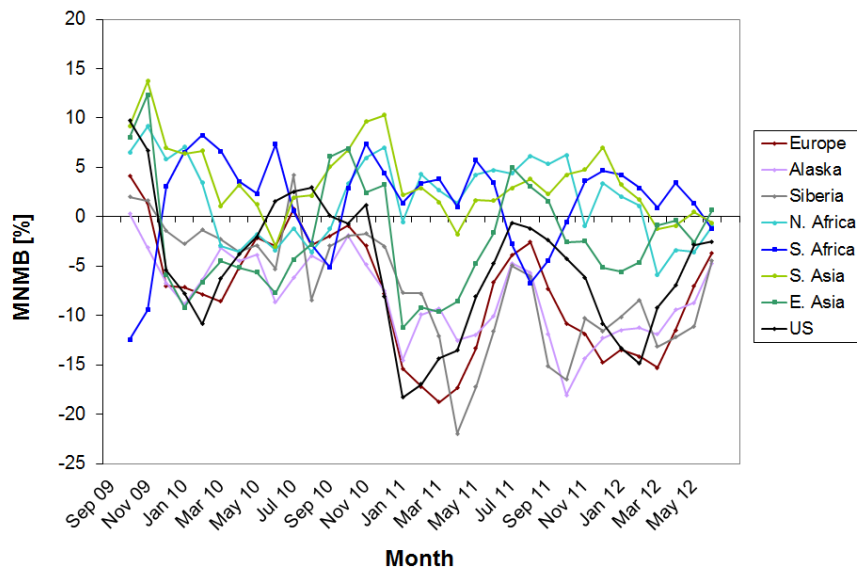
1

2   Figure 13: Monthly average of modified normalized mean biases (MNMBs) derived from the

3   comparison of the MACC_osuite with MOPITT CO total columns for 8 different regions

4   during the period 09/2009 to 06/2012 (see legend on the right).
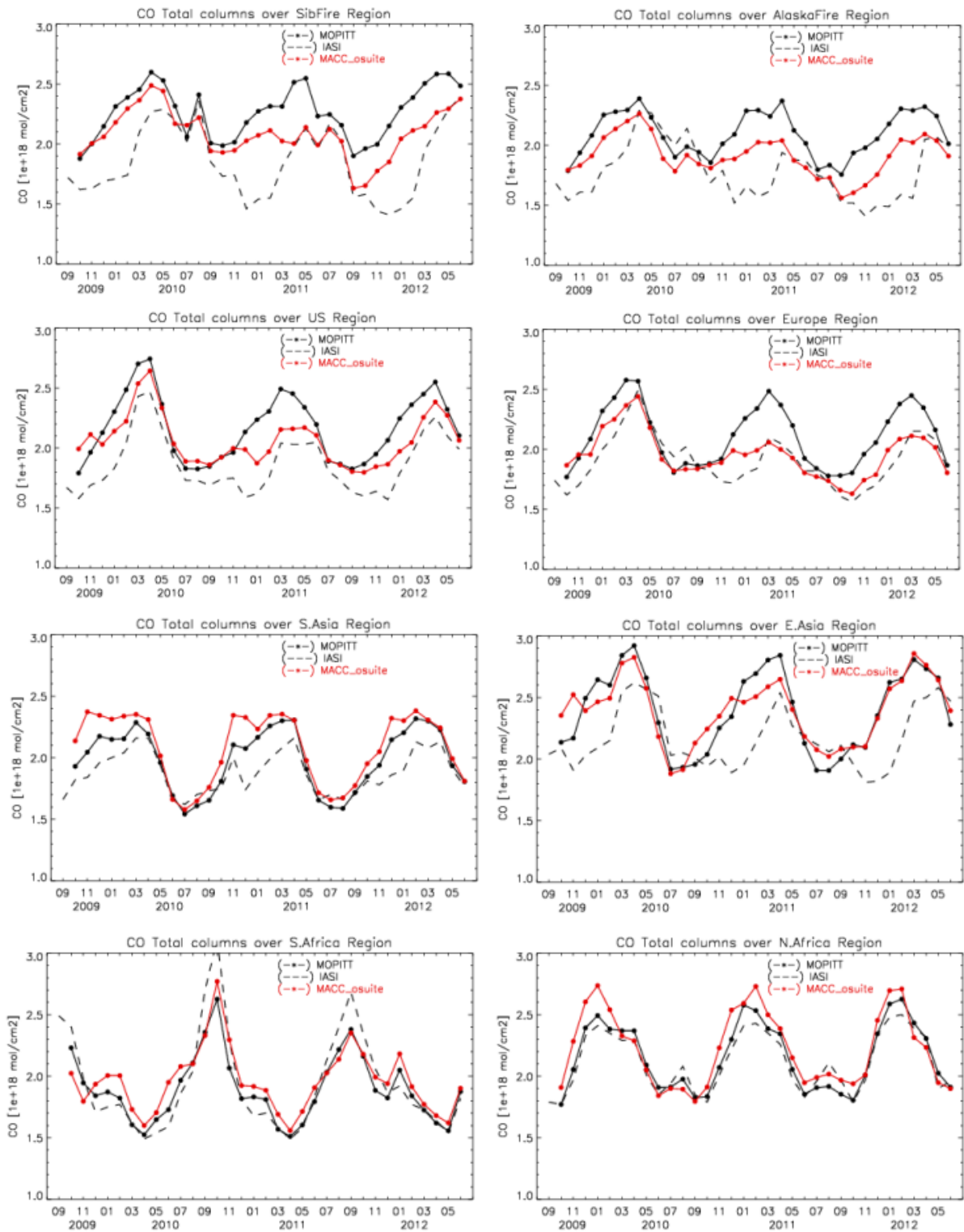
1

2
3   Figure 14: Time series plots of MOPITT CO total columns (black line) compared to IASI CO

4   total columns (black dashed line) and the MACC_osuite CO total columns (red line) for 8

5   different regions (defined in Figure 1) during the period 09/2009 to 06/2012. Top: Siberia

6   (left), Alaska (right), second row: United States (left), Europe (right), third row: South Asia

7   (left), East Asia (right) bottom: South Africa (left), North Africa (right).
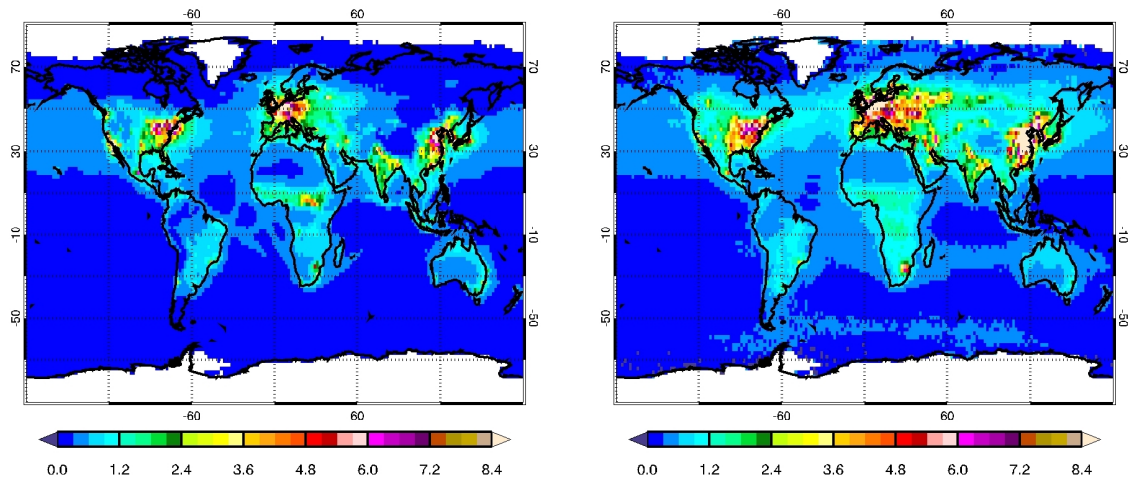
1

2   Figure 15: Long-term average of daily tropospheric NO_2 VCD [10^{15} molec cm^{-2}] from

3   September 2009 to March 2012 for (left) MACC_osuite simulations and (right)

4   SCIAMACHY satellite observations. Blue colours represent low values; red/brown colours
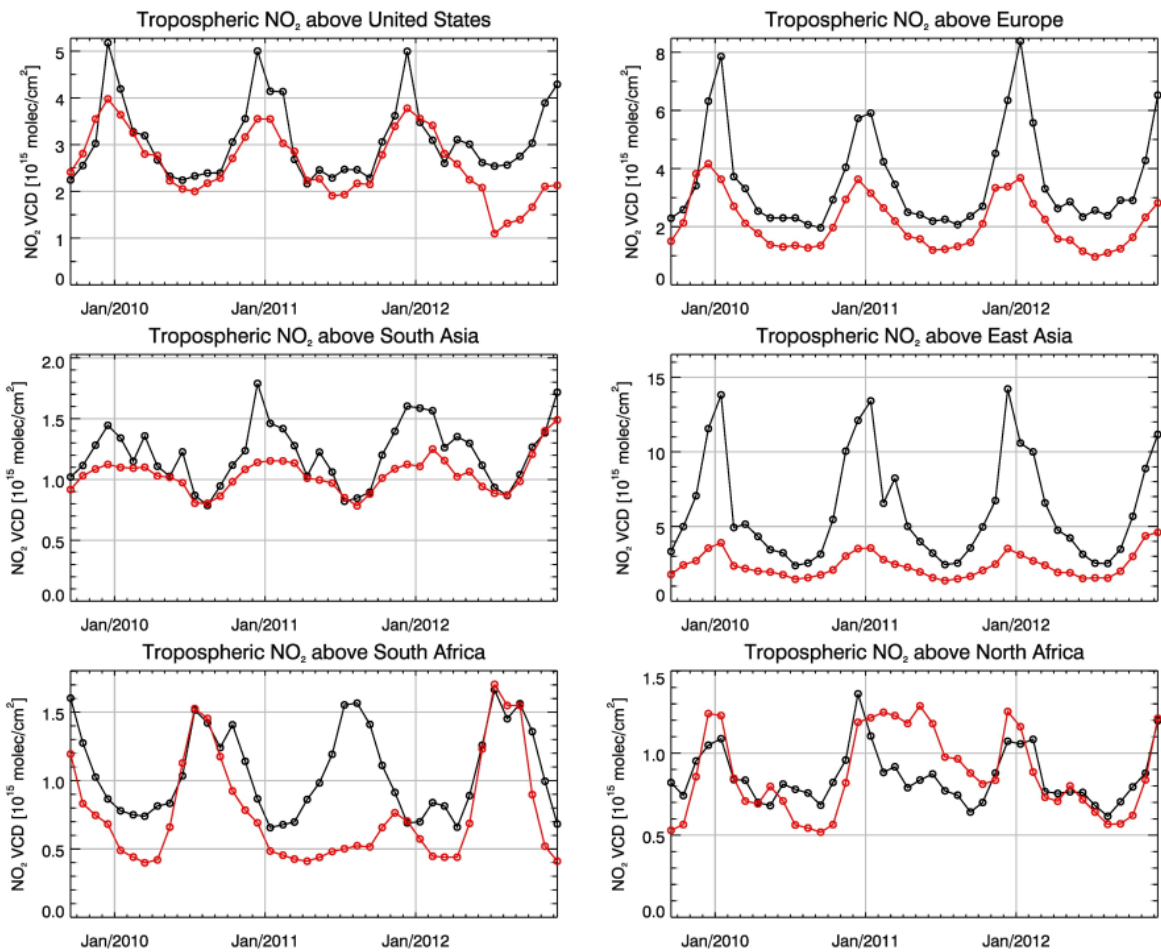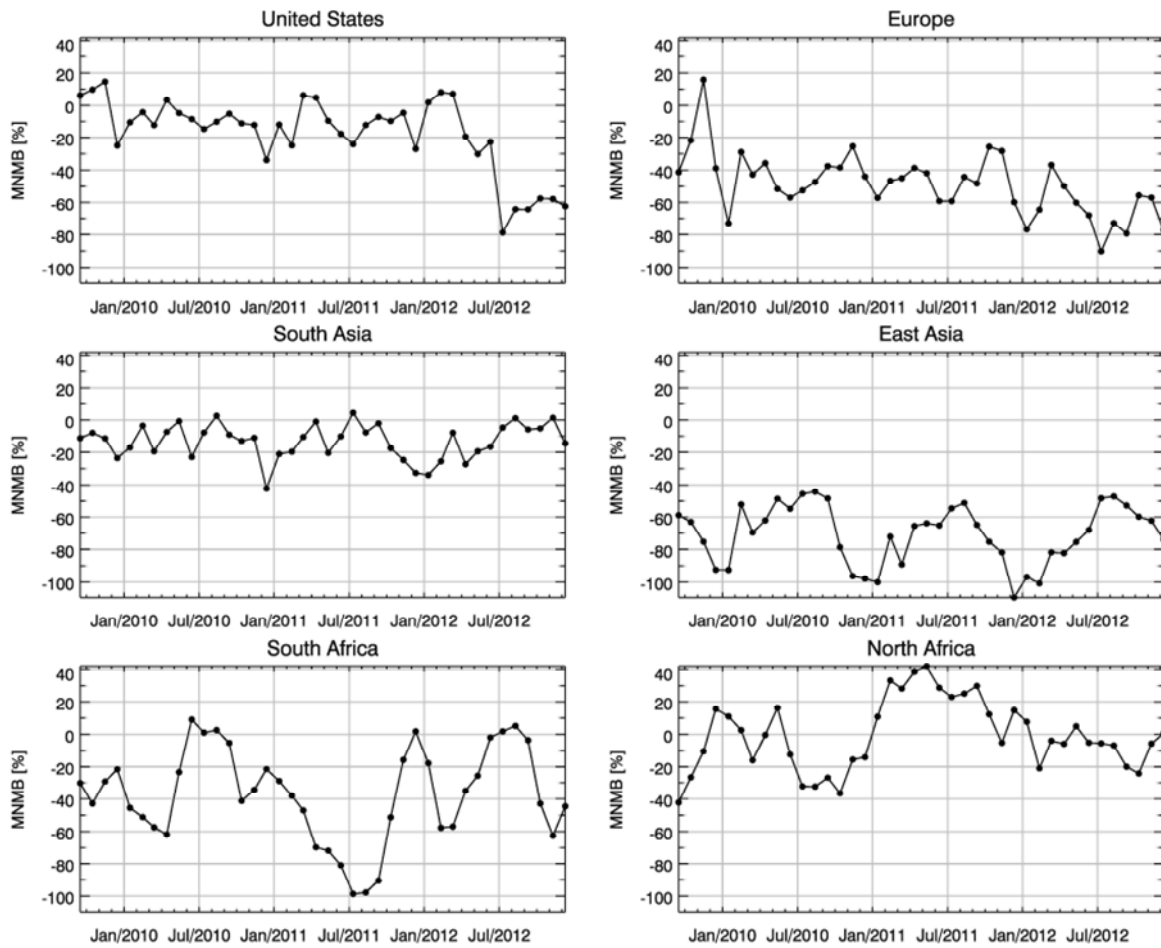
5   represent high values.

1

2
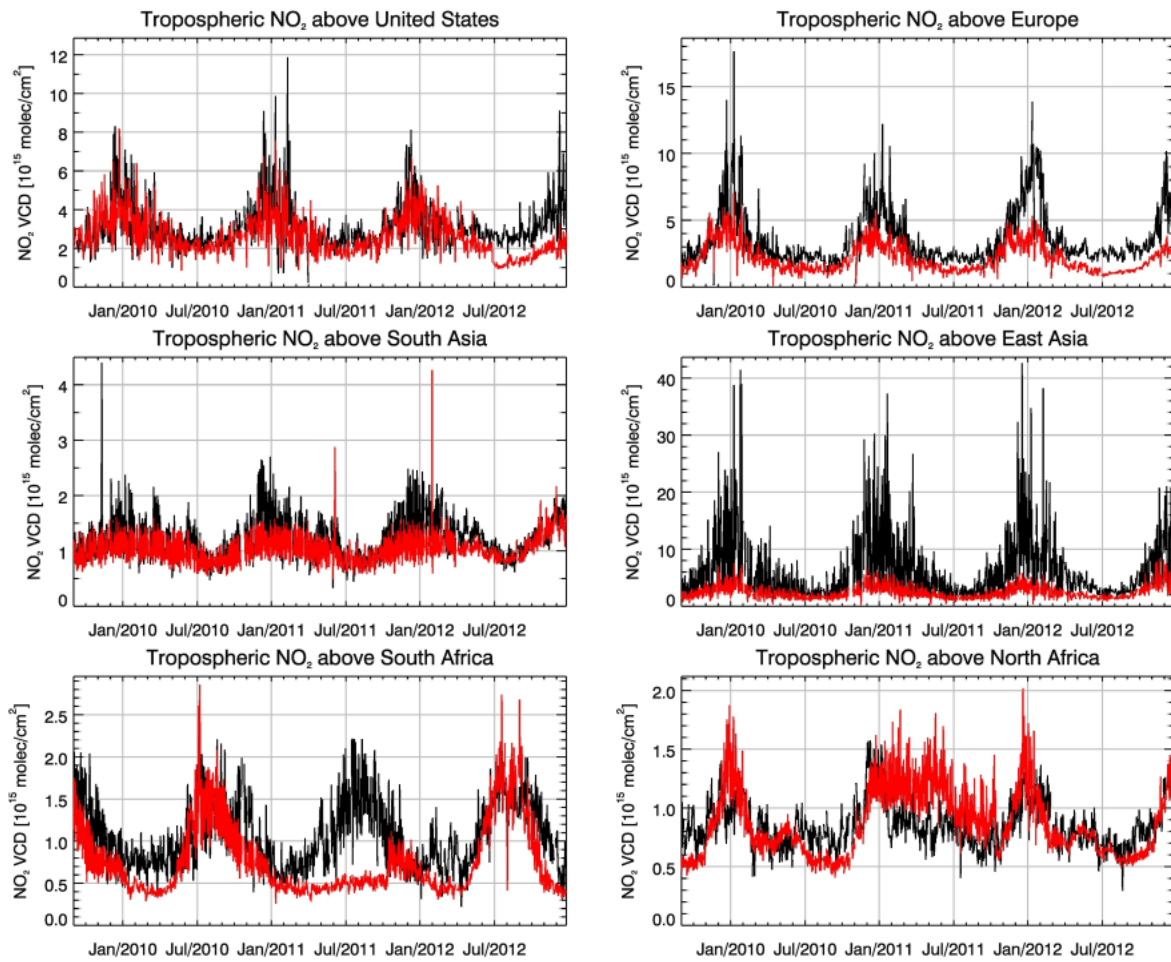
Figure 16: Time series of daily tropospheric NO2 VCD [10^{15} molec cm-2] averaged over
different regions. Top: United States (left), Europe (right), second row: South Asia (left), East
Asia (right), bottom: South Africa (left), North Africa (right). Black lines show satellite
observations (SCIAMACHY up to 03/2012, GOME-2 from 04/2012 to 12/2012), red lines
correspond to the MACC_osuite simulations.

8

Figure 17: As in Fig. 16 but for monthly means of daily tropospheric NO_2 VCD [10^{15} molec cm^{-2}] averaged over different regions. Top: United States (left), Europe (right), second row: South Asia (left), East Asia (right), bottom: South Africa (left), North Africa (right).

Figure 18: Modified normalized mean bias [%] for monthly means of daily tropospheric NO_2 VCD averaged over different regions (see Fig.1 for latitudinal and longitudinal boundaries) derived from the MACC_osuite simulations and satellite observations (SCIAMACHY up to 03/2012, GOME-2 from 04/2012 to 12/2012). Top: United States (left), Europe (right), second row: South Asia (left), East Asia (right), bottom: South Africa (left), North Africa (right).Values have been calculated separately for each month.
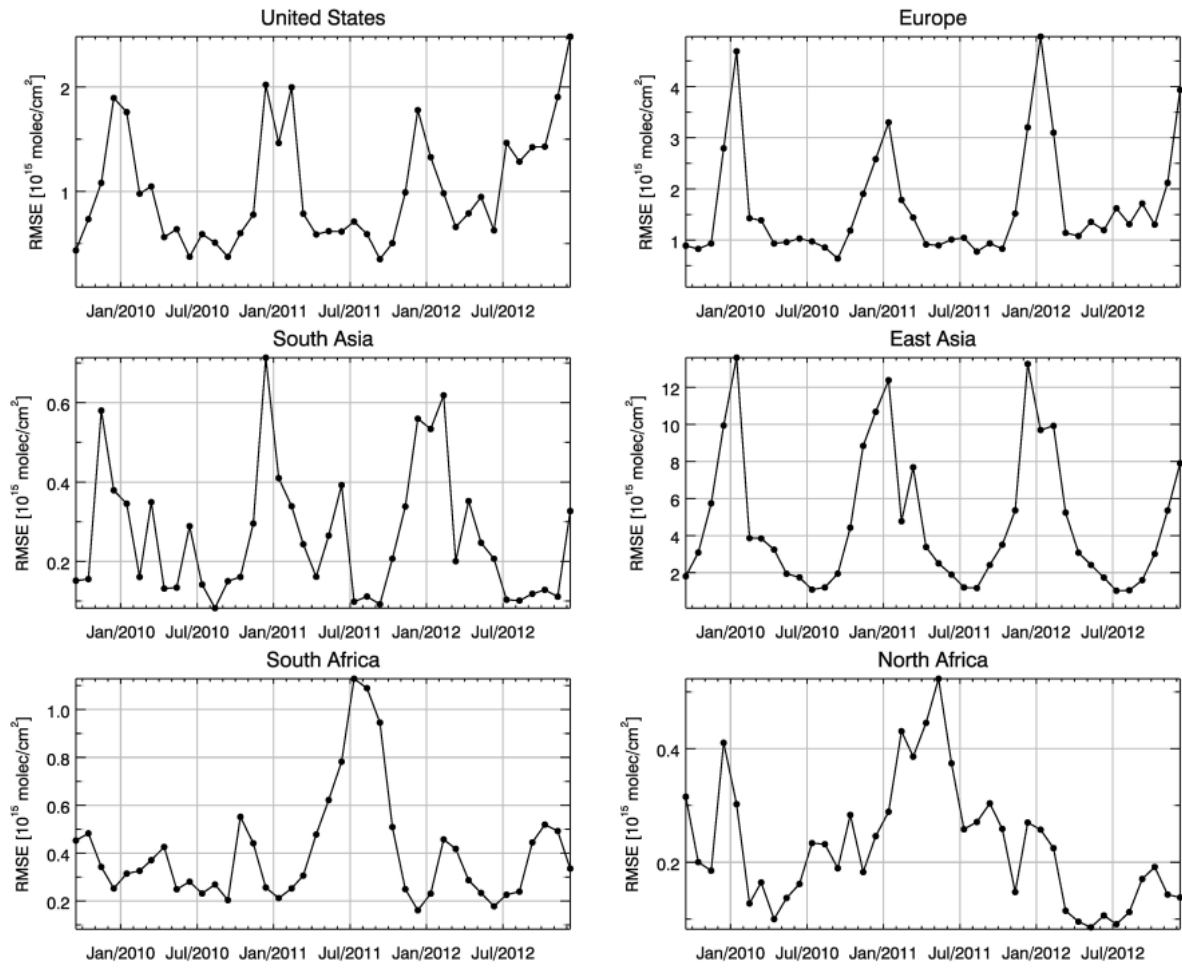
1

2   Figure 19: As in Fig. 18 but for the root mean square error [10^{15} molec cm^{-2}].